DEVELOPMENTS FOR A SWEPT WING AIRFOIL TO STUDY THE EFFECTS OF STEP AND GAP EXCRESCENCES ON BOUNDARY LAYER TRANSITION

A Thesis

by

SIMON PETER HEDDERMAN

Submitted to the Office of Graduate Studies of
Texas A&M University
in partial fulfillment of the requirements for the degree of

MASTER OF SCIENCE

Approved by:

Chair of Committee,	William S. Saric
Committee Members,	Helen L. Reed
	Rodney D. W. Bowersox
	Andrew T. Duggleby
Head of Department,	Rodney D. W. Bowersox

May 2013

Major Subject: Aerospace Engineering

ABSTRACT

Skin friction drag reduction is one of the most promising paths in the investigation of the reduction of aircraft fuel burn. 40 – 50% of overall drag comes from the surfaces of the wings and stabilizers. Natural laminar flow airfoils can extend the region of laminar flow and reduce skin friction drag. However, real-world aircraft wings do not have perfectly smooth surfaces, and therefore the tolerances for step and gap excrescences on these airfoils must be investigated. Previous work has focused on excrescences on flat plates, and only recently included pressure gradient effects.

A new three-dimensional swept wing airfoil with an actuated leading edge (SWIFTER) has been constructed, and will extend the body of knowledge of step and gap excrescences to a more real-world configuration and higher Reynolds numbers. An integrated control system for the leading edge actuation system is proposed, including both interface hardware and control code. A heating system for the test surface is also discussed, and the controller hardware, sensors, and code specified. For wind tunnel testing, a proposed set of wall liners are developed from zero-lift condition streamlines and divided into parts suitable for manufacturing, assembly, and installation. Finally, preliminary wind tunnel step excrescence tests using an existing swept-wing model and appliqué step material were conducted, and the results are discussed with relevance to testing on the new model.

DEDICATION

To my parents, Eamon and Avril Hedderman. I would never have made it this far without your constant support and encouragement.

ACKNOWLEDGEMENTS

Firstly, I would like to thank my advisor, Dr. William Saric, for allowing me the opportunity to study at Texas A&M University and to work at the Flight Research Lab. Working and studying here has been one of the best experiences in my life, both in terms of personal and professional development. Dr. Saric has driven my growth as both an engineer and a student, and the knowledge and experience which I have gained as a result of his guidance will serve me well through my career. I would also like to thank the other members of my committee, Drs. Helen Reed, Rodney Bowersox, and Andrew Duggleby for their support, time, and expertise.

I have had the great privilege of working with some outstandingly talented fellow students while at the FRL, and I would like to thank Brian Crawford, Rob Downs, Tom Duncan, Joshua Fanning, Lauren Hunt, David West, Tom Williams, and the Matts various (Roberts, Tufts, Kuester and Woodruff) for their camaraderie, advice, encouragement and toleration of my idiosyncrasies throughout my time here. Many thanks also to Cecil Rhodes, A&P mechanic extraordinaire, and the man that keeps the Flight Lab flying. Working alongside him has been hugely enjoyable, and has massively expanded my knowledge of how airplanes work (and sometimes don't!). Many thanks also to Colleen Leatherman, without whom nothing would ever happen on time or efficiently in the group.

Having two vastly experienced test pilots working at the Flight Lab has taken me from no knowledge of crew and flight operations to where I am today, and for that I am grateful to Aaron Tucker and Lee Denham. Aaron took the time to share his knowledge of test procedures, crew resource management and flight operations, and has played a leading role in making our test operations as safe and professional as they have become. Thanks also to Lee for his ever present enthusiasm, and for putting me on a path to gaining my pilot's license. Both he and Aaron are natural teachers, and the time they gave to patiently leading me through the basics of controlling an aircraft is appreciated enormously.

Finally, I would like to thank my family and friends. Their constant support and encouragement throughout my time here has kept me motivated through it all, even on the days when the light at the end of the tunnel started to look more like an oncoming train. On a similar note, thanks to the creators of Skype. I owe you my sanity.

NOMENCLATURE

C_l	Coefficient of lift
C_p	Coefficient of pressure
C_p	Specific heat
DAQ	Data AcQuisition
FoS	Factor of Safety
FRL	Flight Research Laboratory
FTE	Flight Test Engineer
h	Dimensional excrescence height
HART	Hyuga Aerodynamic Research by Towing
IR	Infrared
K	Pressure parameter
k	Dimensional excrescence height
KIAS	Knots Indicated Air Speed
KSWT	Klebanoff Saric Wind Tunnel
LSWT	Low Speed Wind Tunnel
m	Mass
MATLAB	MATrix LABoratory
MEATLOAF	Manufacturing Tolerances for Laminar Flow
MOSFET	Metal Oxide Semiconductor Field-Effect Transistor
NACA	National Advisory Committee for Aeronautics

NLF	Natural Laminar Flow
NTS	Non-Test Surface
OML	Outer Mold Line
P	Power
PID	Proportional Integral Derivative
PTFE	PolyTetraFluoroEthylene
Re_k	Non-dimensional excrescence height
Re_{kcrit}	Non-dimensional critical excrescence height
Re_{tr}	Non-dimensional transition location
Re_{xk}	Non-dimensional chordwise location of excrescence
R_{hcrit}	Critical excrescence height based on h
RMS	Root Mean Square
RPM	Revolutions Per Minute
RTD	Resistive Temperature Detector
SETS	Surface Excrescence Transition Study
SSR	Solid State Relay
SWIFT	Swept Wing In-Flight Test
SWIFTER	Swept Wing In-Flight Test Excrescence Research
t	Time
T_f	Final temperature
T_i	Initial temperature
TS	Test Surface

T-S	Tollmein-Schlichting instability
U_e	Boundary layer edge velocity
U_k	Velocity at excrescence height
U_∞	Freestream velocity
VI	Virtual Instrument
β	Pressure parameter
β	Model Angle of Attack/Aircraft Yaw Angle
v	Kinematic viscosity
v_k	Viscosity at excrescence height

TABLE OF CONTENTS

Page

LIST OF FIGURES

CHAPTER I

INTRODUCTION

Motivation

With current economic pressures and fast-dwindling oil reserves, both commercial airlines and military aviation services see fuel burn reduction as a major priority. There are several avenues of improvement being investigated, including increased-efficiency engines, higher-energy-density fuels, the use of lightweight composite structures in airframe construction, improved aerodynamic efficiency, more efficient flight routing, and local air traffic control.

One of the promising development avenues in the improvement of aerodynamic efficiency is that of aircraft skin friction drag reduction. On a modern airliner, turbulent skin friction is responsible for 50% of the overall drag budget (Figure 1), and even more on business jet type aircraft (Saric 2010). Contributions to the skin friction drag come largely from the fuselage, but 40-50% of the total comes from the surfaces of the wings and the vertical and horizontal stabilizers.

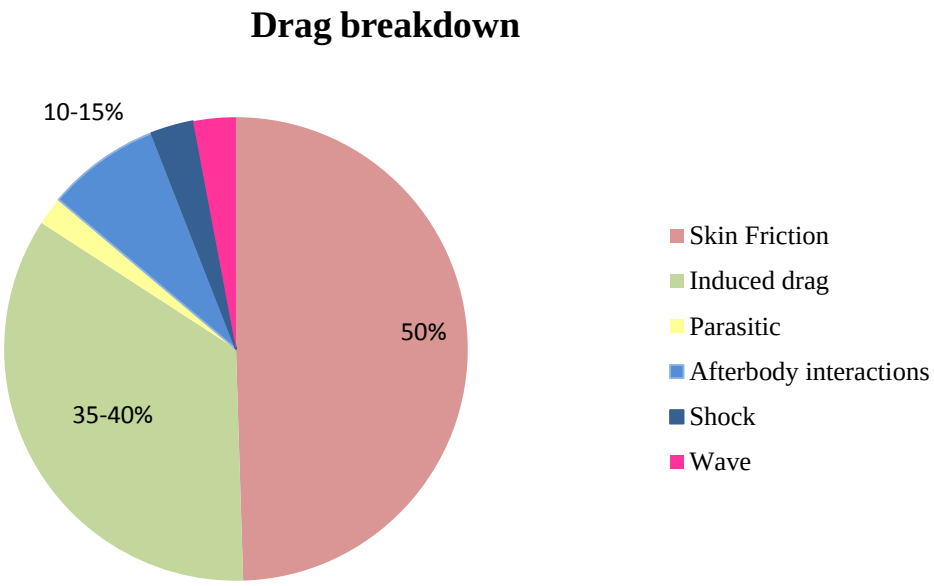

Figure 1 - Drag breakdown on a modern airliner

Extending the region of laminar flow, with its lower coefficient of friction, can see significantly reductions made in the total drag – up to 15%. This can then translate to significant fuel burn savings, which would result in very large cumulative financial savings across an entire fleet. However, the implementation of laminar flow design into aircraft has proved difficult. Designing an airfoil suitable for extended laminar flow requires an outer mold line (OML) that is quite different from traditional airfoils in order to control disturbances in the boundary layer and delay the transition of the flow to turbulence.

This must be balanced, however, with the performance requirements of the aircraft, as laminar flow airfoils can have lower coefficients of lift (*Cl*), which may lead to limitations on the design of the aircraft as a whole. Moreover, the manufacturing tolerances for the surfaces of laminar flow airfoils, particularly in the leading edge region, are much more restrictive than traditional airfoils, both in terms of overall surface finish, and in the acceptable sizes of steps and gaps, which are almost unavoidable on production aircraft. All of this leads to cost and time increases, not just in the initial manufacturing stages, but also in the ongoing maintenance of the surface, which can significantly reduce the potential savings from the design, and tend to be off-putting to manufacturers. As the tolerance requirements for these surface excrescences are not yet fully understood, current guidelines may be tighter than necessary to maintain the benefits of the design. If it was found that these tolerances could be loosened, and a correlation between step height or gap width and transition location was developed that was based on a criteria applicable to a wide range of airfoil designs and flight conditions, cost savings would follow, as

a) The cost of manufacturing and surface maintenance would drop,

b) Testing each specific new design would no longer be required, and

c) The criteria could be used to make appropriate decisions about the location of unavoidable steps and gaps, such as maintenance hatches and deicing equipment.

Literature Review

Though there is a large body of work on the effect of step and gap excrescences on transition to turbulence, the majority of existing data are for flat plates with zero to a very mild positive pressure gradient. One area that had not been investigated in the literature until recently was the effect of pressure gradients on transition in the presence of step and gap excrescences, particularly in the region of the leading edge of the airfoil. A favorable pressure gradient has a stabilizing effect on a boundary layer, which delays transition, and would theoretically allow larger step and gap excrescences than in a zero gradient scenario. This would suggest that the criteria and guidelines established previously are inherently conservative for natural laminar flow (NLF) airfoils, being based in large part on flat plates with no pressure gradient data, while NLF airfoils tend to have favorable pressure gradients over their leading edge regions. This leads to very restrictive manufacturing tolerances for practical aircraft design as seen in Drake et al. (2010), which took the case of an example aircraft designed for high altitude and long endurance, with chord of 1.52m, Mach 0.6, and altitude of 55,000 feet (Figure 2). Forward-facing steps are limited to the order of 250μm, and aft-facing steps even smaller, in the absence of consideration of a pressure gradient.

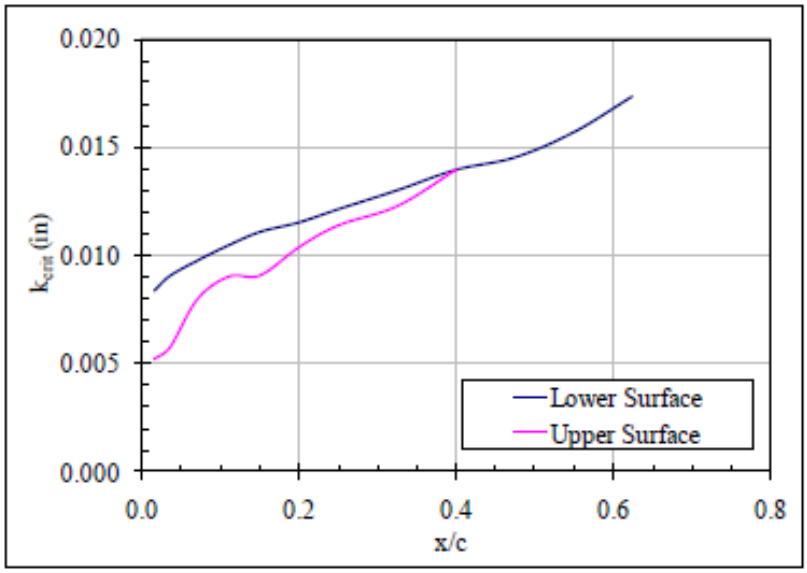

Forward-facing step on a long-endurance aircraft.

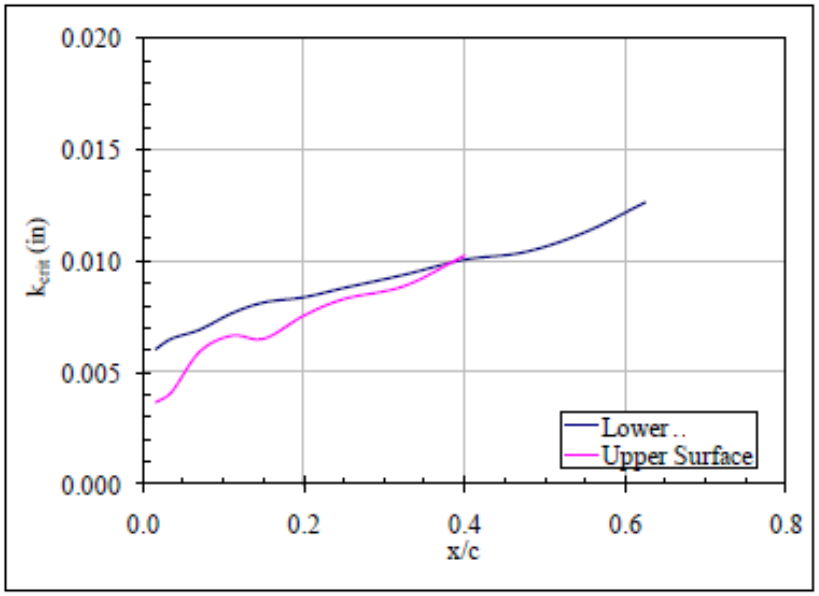

Aft-facing step on a long-endurance aircraft.

Figure 2 - Step excrescence tolerances (Drake et al., 2010)

Pioneering work in this area was conducted by Aaron Drake and Anne Bender at Northrop Grumman, investigating step and gap excrescences on two-dimensional airfoils with favorable pressure gradients over a wide range of chord Reynolds numbers and excrescence sizes. This thesis describes work done in preparation for a follow-on study of the effect of step and gap excrescences on transition to turbulence on a three-dimensional swept-wing. The study will comprise both wind tunnel testing in the ultra-low disturbance Klebanoff-Saric Wind Tunnel (KSWT), and flight testing at the Texas A&M Flight Research Laboratory (FRL), mounted to the lab's Cessna O-2A experimental platform. The tests will be conducted with a newly-constructed airfoil model with an actuated leading edge to produce forward-facing and aft-facing steps, gaps, and combinations of the above.

In any discussion of flow involving step excrescences, the common parameters must be defined. First, the excrescence height can be non-dimensionally expressed as an excrescence Reynolds number, Re_k, where

$$Re_k = {u_k k}/{\nu_k}$$

and u_k is the velocity at the excrescence height k above the surface, and ν_k is the viscosity at the same height. The literature refers to the allowable step tolerance in terms of a non-dimensional critical step height, or Re_{kcrit}, which allows a comparison across a broad

range of situations. Works such as Drake et al. (2008) use the parameter *K* to describe the non-dimensionalized pressure gradient, as they regard it as a parameter "readily available to the aerodynamic designer", while acknowledging that it is not ideal for more in-depth studies. *K* is defined in Zhou and Wang (1992) as

$$K = \frac{\nu}{U_e^2}\frac{dU_e}{dx} = \frac{\mu}{\rho U_e^2}\frac{dU_e}{dx}$$

Issues arise with this definition of pressure gradient when accelerated flows over steps or ramps are considered. The presence of a viscosity term in a description of an inviscid phenomenon, as well as the fact that if temperature changes, but all other factors are held constant, *K* will change, but the pressure gradient will not, suggest that the Hartree parameter, β, would be more appropriate for these flows. The Hartree parameter, based on the Falkner-Skan solution for similarity flows, is defined as

$$\beta = \frac{2}{U_e^2}\frac{dU_e}{dx}\int_0^\infty U_e dx$$

where

$$\beta = \frac{2m}{m+1} \; for \; U_e = cx^m$$

In the literature, focus has primarily been on surface excrescences comprising forward facing steps, raised strips or ridges, wires, bulges and waves, with some attention also paid to isolated aft facing steps. Early work by Fage (1943) looked at the effects of ridges on the surface of airfoils. These ridges consisted of a forward facing step, followed 2.54cm further downstream by an aft facing step. The conclusions reached were that neither shape of the excrescence, nor the pressure gradient, had much influence on the critical height. However, this may have been as a result of the particular shapes tested. For a ridge excrescence, a laminar separation bubble is created both at the forward and aft facing steps on the upstream and downstream sides of the ridge. Therefore, any resultant effect on transition can be viewed only as coming from a combination of the two separated regions. Fage expressed his tolerances in terms of a relationship between the excrescence geometry, boundary layer edge velocity, kinematic viscosity, and transition location, which became known as the Fage Criterion. A Re_{kcrit} value of 900 can, however, be extracted from the data (Drake et al, 2010).

Later similar work by Drake et al. (1996) investigated combinations of ridges and gaps, but this time in a flight environment, at Mach 0.5 to 0.8. The purpose of the experiment was to study the possibility of smoothing the interface between the removable leading edge of a business jet and the primary wing surface with a strip insert.

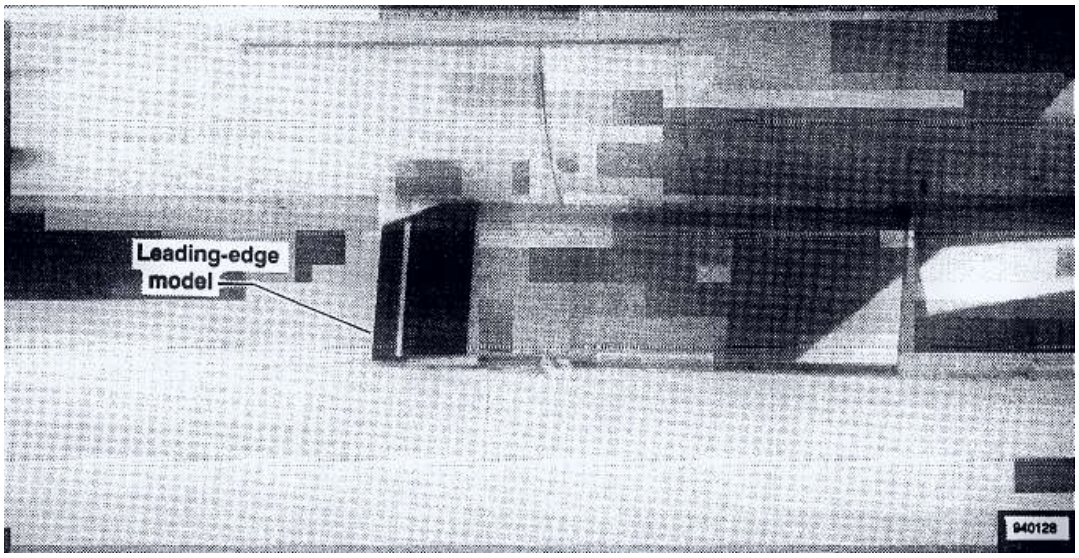

Figure 3 - Test airfoil on underside of F-104G aircraft (Drake et al., 1996)

The airfoil under test was mounted to the underside of an F-104G aircraft on a specific flight test fixture (Figure 3). It had a favorable pressure gradient to attempt replicate a natural laminar flow design. Several configurations were tested, and those with a forward-facing step, followed one inch downstream by an aft-facing step, gave a Re_{kcrit} value of about 500.

Obara and Holmes (1985), discusses testing on both the NASA X-21A and T-34C experiments. The critical Reynolds number in these cases, $R_{h,crit}$ was determined based on freestream velocity U_∞, kinematic viscosity ν, and the height of the step or length of the gap, h.

$$R_{h,crit} = {}^{U_\infty h}/_{\nu}$$

The X-21 tests investigated the effect of forward-facing steps in the leading edge region of the wings on transition. In addition to this, the effect of gaps was studied at the nose of the aircraft. Forward-facing sharp steps were found to have a $R_{h,crit}$ value of 1800, while gaps were found to have a $R_{h,crit}$ value of 15,000 (The literature does not state whether streamwise or leading edge normal definition was used to determine critical Reynolds numbers for these excrescences). This suggests that gaps have far less of an influence on transition than steps. Later tests investigating the effects of steps on transition were conducted using an NLF glove on the unswept wing of a T-34C Turbo-Mentor aircraft. Steps were located near the leading edge of the lower side of the glove, with a mild favorable pressure gradient. It was found that for the sharp forward facing steps, the $R_{h,crit}$ value was 1800. However, for the rounded forward-facing steps, the transition location was well downstream from the step, giving a $R_{h,crit}$ value of 2700 (Figure 4). This can be attributed to the smaller separation bubble generated by the less-severe geometry change of the rounded step. Additional tests were conducted to

investigate steps over a range of sweep angles. However, these tests would not be an accurate representation of swept-wing step excrescence effects, as the airfoil itself was not swept, and not subject to as large a degree of crossflow instability.

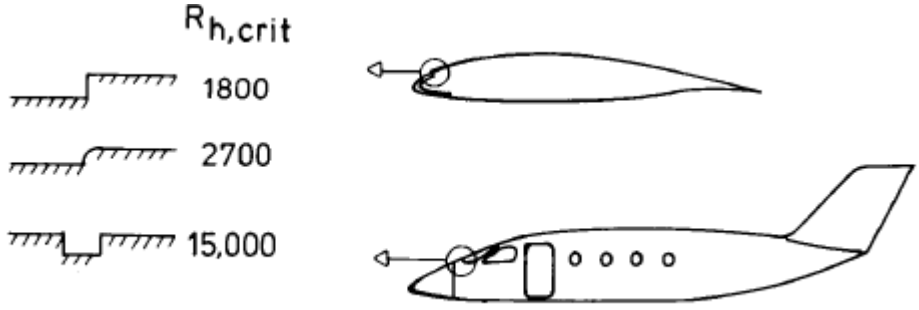

Figure 4 - X-21 & T-34C testing critical Reynolds numbers (Obara & Holmes, 1985)

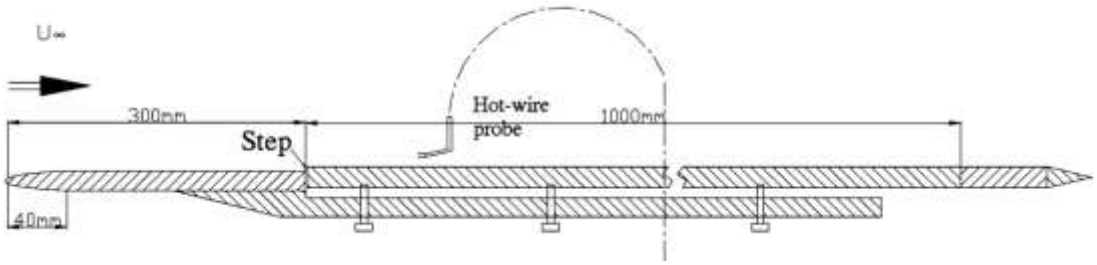

Figure 5 - Flat plate step excrescence study setup (Wang and Gaster, 2005)

Wind tunnel tests on flat plates with forward-facing and aft-facing steps (Figure 5) have also been conducted by Wang and Gaster (2005), and Crouch et al (2006). These experiments both found that an aft-facing step was two to three times more effective at causing transition to turbulence than a forward-facing step. Drake et al (2010), suggests that an Re_{kcrit} value for aft-facing steps could be extrapolated from that for a wire trip (Re_{kcrit} = 120), of which there is more data in the literature. Taking into account the lack of compression before the step that would have occurred with a wire trip, and had a stabilizing effect on the boundary layer, an Re_{kcrit} value of 80 is estimated.

To develop a relationship between pressure gradient and $Re_{kcrit,}$ Northrop Grumman Corporation began research on flat plates with favorable pressure gradients under the Surface Excrescence Transition Study (SETS), with first results published in Bender et al (2005). Initial testing was conducted at Washington State University, in the Contractionless Boundary Layer Wind Tunnel (Figure 6). This is an open loop tunnel, with a 1.82m long, 0.61x0.61m test section, and unit Reynolds number up to $0.66x10^6$/m. The test section has a flexible upper wall, allowing varying pressure gradients to be set. The test model was a 1.22m chord flat plate with a super ellipse leading edge, and was made in two pieces, allowing a step to be created 0.23m aft of the leading edge (Figure 7). This low-speed testing showed that transition location did change as a result of varying the pressure gradient on the model, and had the potential to loosen manufacturing tolerances. However, the data was limited by the maximum achievable chord Reynolds number of roughly $7.5x10^5$, and tunnel freestream turbulence levels were not ideal for this testing, so a different facility was required for further investigation.

Figure 6 - Contractionless Boundary Layer Wind Tunnel (Bender et al., 2005)

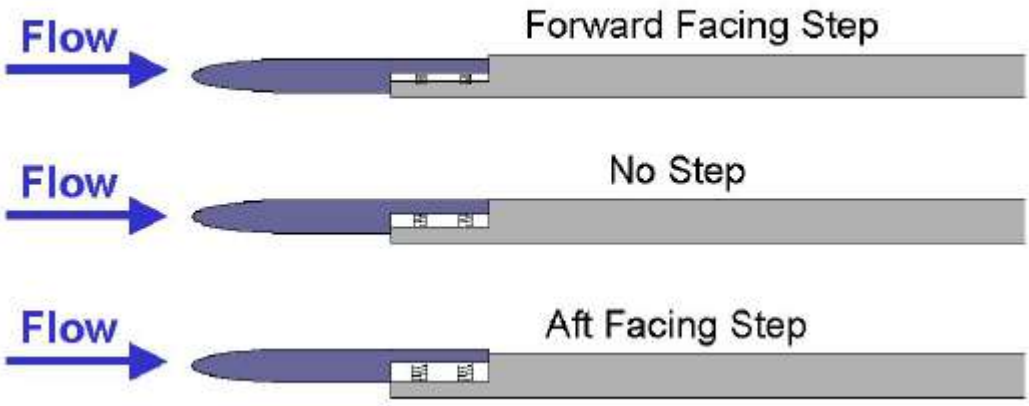

Figure 7 - Northrop flat plate model step design (Bender et al., 2005)

The facility selected was the Tohoku University Towing Wind Tunnel in Japan (Figure 8). It consists of a 2km long test track, on which an electric vehicle, known as the Hyuga Aerodynamic Research by Towing (HART) vehicle, runs. The model under test is placed on the vehicle, accelerated, and then studied in a 515m long covered measurement region. The maximum speed of the vehicle is 50m/s. Initial tests at this facility were conducted with a model identical to that used in the low speed testing, giving a maximum chord Reynolds number increase of roughly five times. The pressure gradient with this flat plate was very mildly favorable. The results of these tests were dramatic. From the low speed testing, an increase in the Re_{kcrit} values was expected, but, as can be seen in Figures 9 & 10, which plot Re_k against Re_{tr}-Re_{xk}, the non-dimensional transition location aft of the step, for both the low-speed tests (Task 1) and the Towing Wind Tunnel data (Task 6), the jump was significant. As expected from the previous literature, the Re_{kcrit} values of aft-facing steps were on the order of two to three times smaller than the forward-facing steps.

Figure 8 - Flat plate test at the Towing Wind Tunnel (Bender et al., 2007)

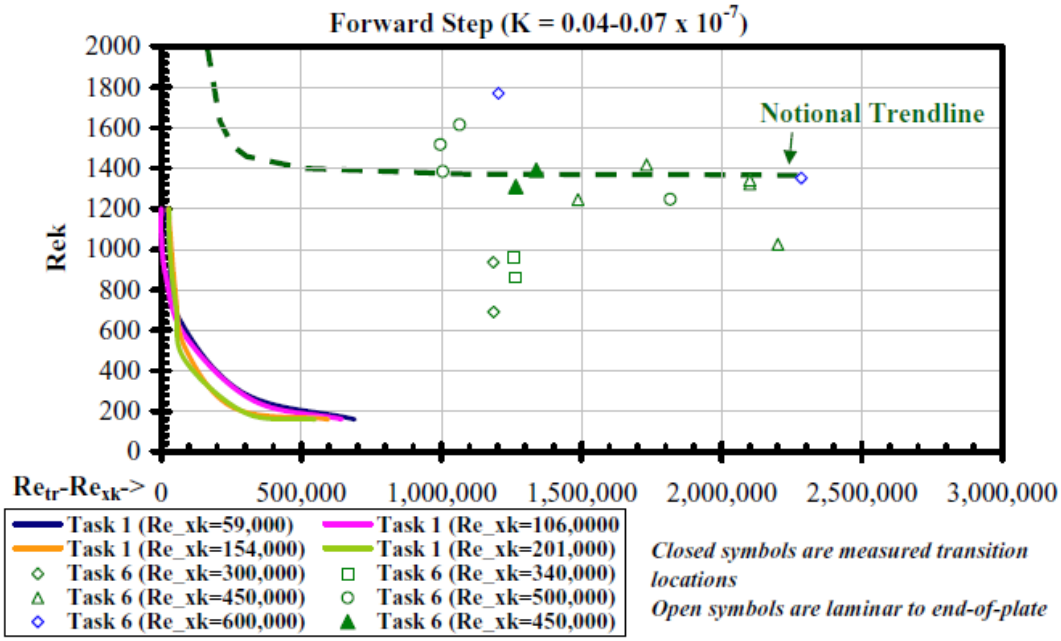

Figure 9 - Forward-facing steps v transition location (MEATLOAF Final Report, 2006)

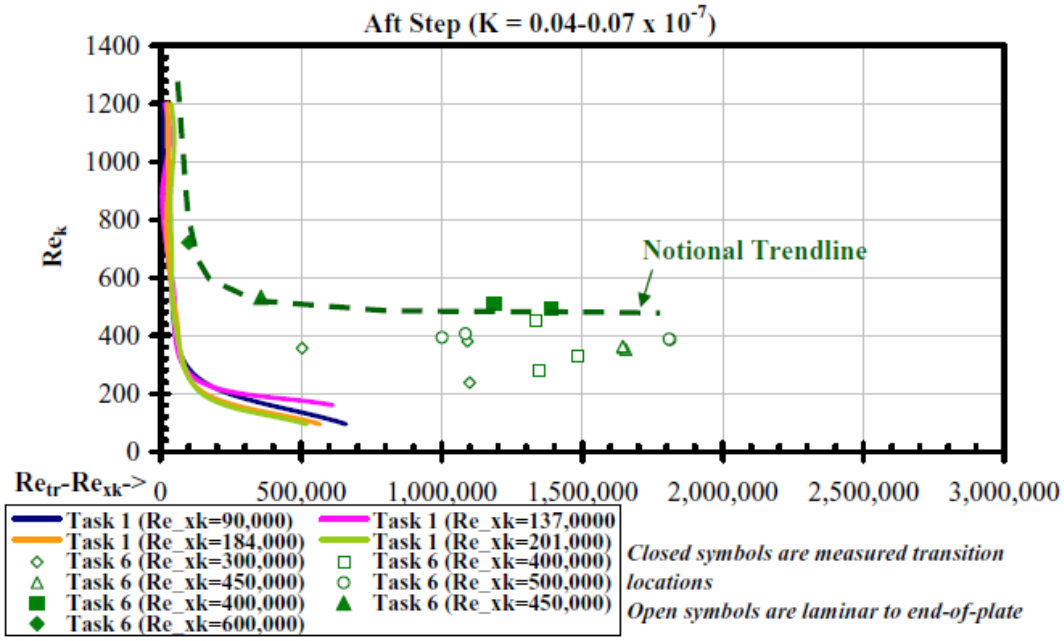

Figure 10 - Aft-facing steps v transition location (MEATLOAF Final Report, 2006)

This increase over the initial low-speed tests can be attributed to the much lower turbulence environment of the open-air test track, which is also much more representative of the flight environment. Later measurements at the facility (SETS Final Report, 2009) found turbulence intensity levels to be 0.05-0.1%, which are closer to the data from Fanning (2012), which measured freestream turbulence levels from the Flight Research Lab's Cessna O-2A platform to be on the order of 0.023-0.047%. This suggested that environmental conditions have a larger influence on excrescence tolerances than was expected, and that further increases will be found in flight testing.

Further studies were conducted using three purpose-built models, (Figure 11), for the Towing Wind Tunnel. One with a nominally zero pressure gradient (Gradient-Z), and two with increased favorable pressure gradients (Gradient-A and Gradient-B) (Figure 12), and variable steps located 0.48m aft of the leading edge along the surface.

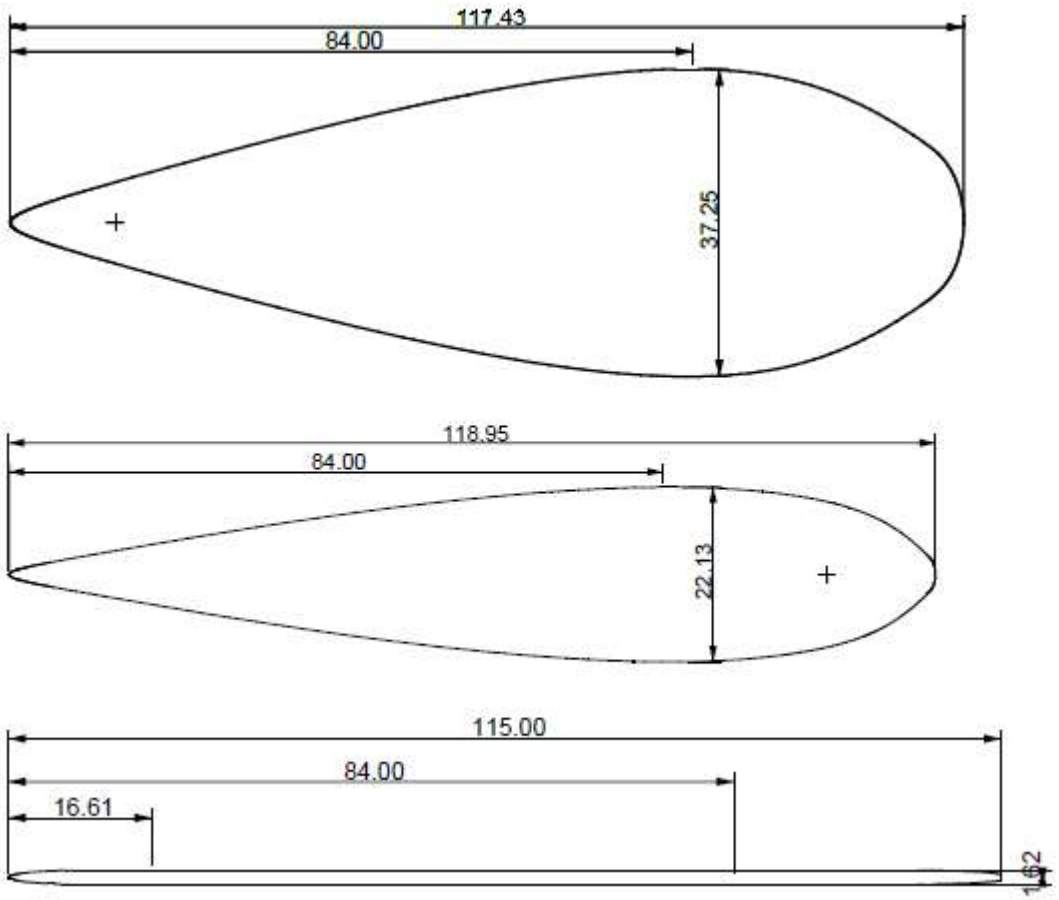

Figure 11 - Gradient-B, Gradient-A, Gradient-Z. Flow is L-R (SETS Final Report, 2009)

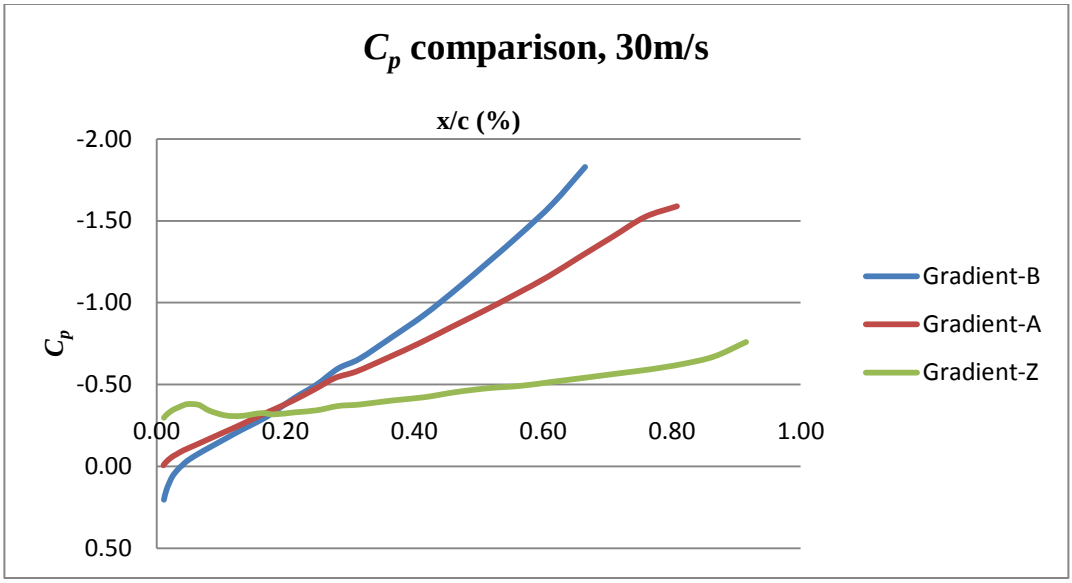

Figure 12 - Comparison of C_p distribution

The longer chord length of the models allowed the chord Reynolds number to be increased to between $4x10^6$ and $8x10^6$ – values much more representative of an aircraft wing in a flight environment. During the testing, issues were encountered with the sealing of the step junction on the Gradient-B model. Therefore, the data from it had significant run-to-run variation, and will not be discussed in this review. The results of testing with the Gradient-Z and Gradient-A models in the Towing Wind Tunnel are shown in Figures 13 and 14 for forward-facing and aft-facing steps, respectively.

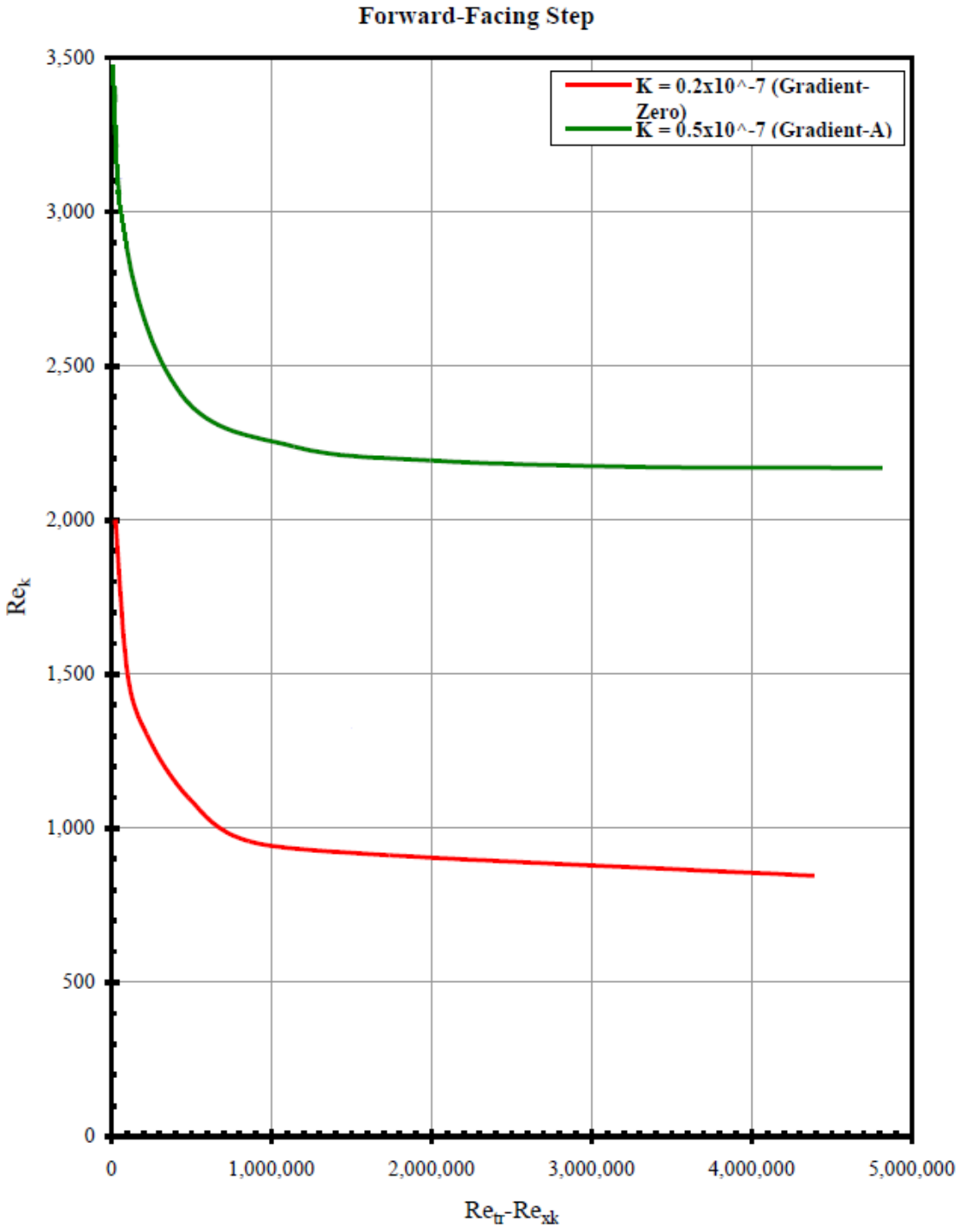

Figure 13 - Forward-facing steps v transition location (SETS Final Report, 2009)

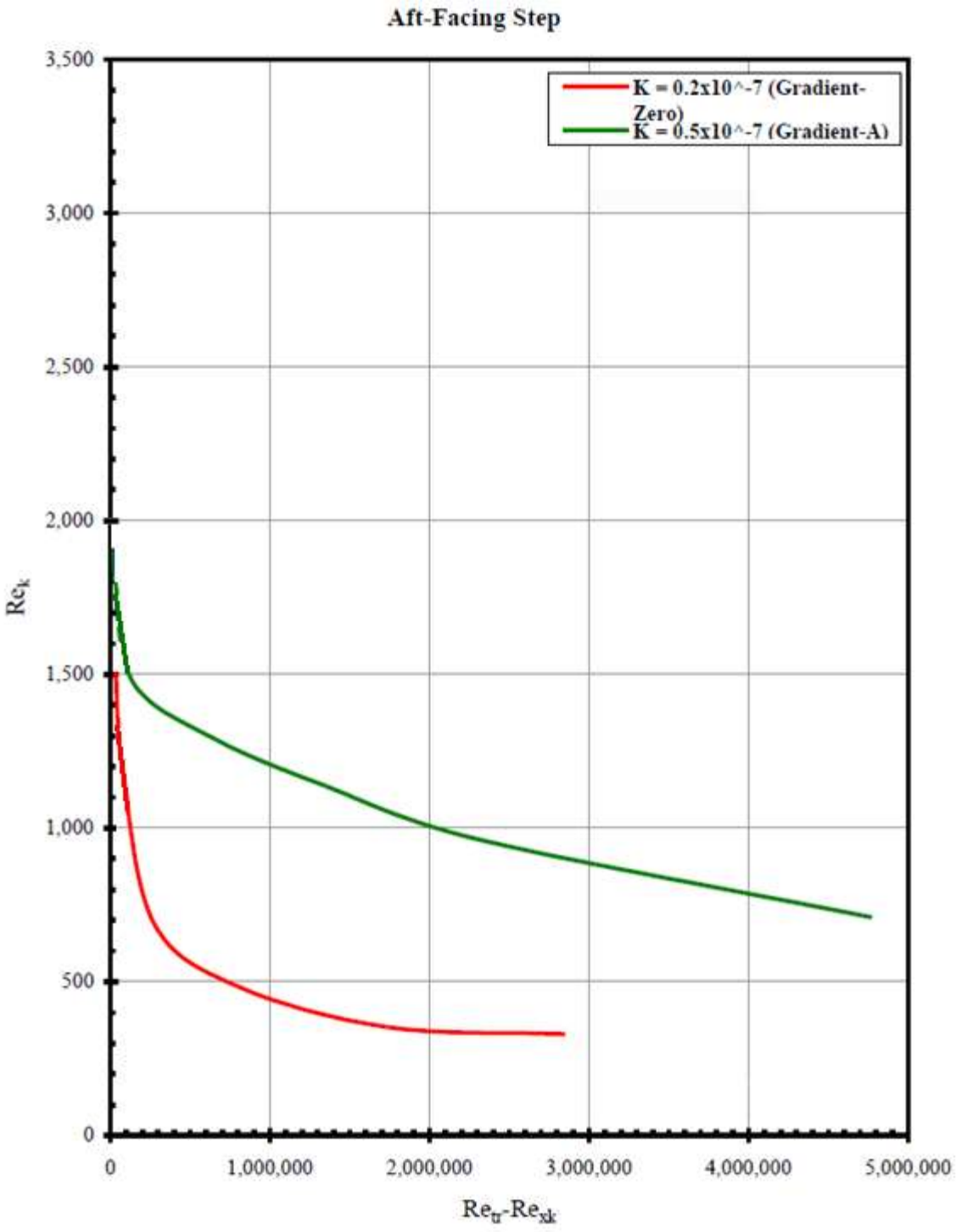

Figure 14 - Aft-facing steps v transition location (SETS Final Report, 2009)

The Gradient-Z data shows much the same results as the initial MEATLOAF Task 6 tests at the facility, but extends the Reynolds number range to over $4x10^6$ at transition. The resulting values of Re_k are slightly lower for both forward-facing and aft-facing steps, but this could be attributed to the pressure gradient being closer to zero on the new model than the original. It was found that transition on both models was linearly caused by the generation of Tollmein-Schlichting (T-S) waves, as would be expected for an unswept flat plate. Comparing the Re_k values of the Gradient-Z and Gradient-A models shows clearly that the increased favorable pressure gradient of the Gradient-A model had a strong stabilizing effect on the boundary layer, and a resultant increase in the excrescence height required to cause transition.

CHAPTER II

EXPERIMENTAL SETUP

Swept Wing In-Flight Testing Excrescence Research (SWIFTER) Model

The SWIFTER model is externally similar to the SWIFT model. It has a leading edge sweep of 30 degrees, and a chord of 1.37m (54 inches), which allows a maximum Reynolds number of $7.5x10^6$ at the maximum dive speed of the O-2A. It has a span of 1.07m (42 inches) at the leading edge, with a 4.5 degree cut aft of the leading edge for ground clearance during takeoff. As with SWIFT, the test surface of SWIFTER aft of the leading edge will be powder coated black to provide an optimal surface for infrared thermography. The outer mold line (OML) of the model is identical to that of SWIFT, with a leading edge symmetric to 15% chord, and the non-test, pressure, surface aft of that designed to cancel any lift generated on the test, suction, surface. The airfoil is designed to generate crossflow instabilities, and be subcritical to T-S waves.

Figure 15 - SWIFTER model

Computational Fluid Dynamics (CFD) analysis by Matthew Tufts, using ANSYS ICEM software, showed that the SWIFT OML would be suitable for this series of excrescence experiments. It can be seen in Figure 16 that the test surface C_p distribution at -4.5 degrees β matched closely with that of the Northrop SETS Gradient A profile, once aft of the leading edge region (SETS Final Report, 2009). This region of the SWIFTER model was never expected to match, due to the large curvature not present on the SETS model.

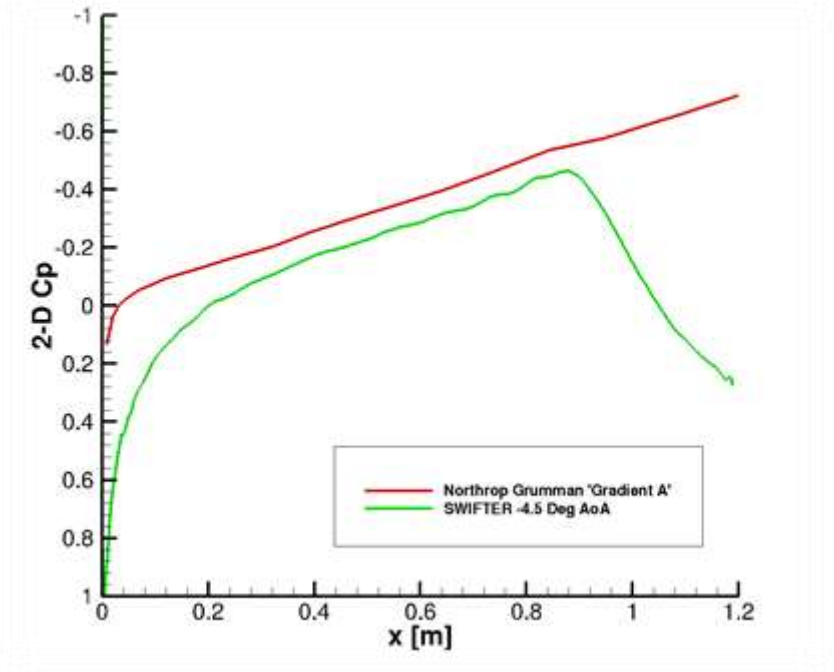

Figure 16 - Comparison of SWIFTER C_p to Northrop SETS Gradient A

The design philosophy of SWIFTER is very similar to that of SWIFT, and a more detailed description of the design of that model can be found in McKnight (2006). Construction is of machined 7075-T6 aluminum, and the model is in three primary sections – the test surface, non-test surface, and leading edge, with a hollow cavity in the center, allowing room for instrumentation. There are, however, some differences in the designs, based both on experimental requirements and on practical considerations, built from several years of operation of SWIFT. With the planned addition of hardware and

instrumentation to allow the leading edge of the model to actuate, and create step and gap excrescences, it was desired that weight be saved in the structure of the model. The primary method by which this was achieved was by replacing the stepped internal faces of the test and non-test surfaces with smooth faces of mainly 3.175mm (0.125 inch) thickness (Figure 17), and a uniform thickness of 6.35mm (0.25 inches) in the leading edge. This was not possible in the construction of SWIFT due to machining limitations. In addition to this, the steel plates at the root and tip of the model on SWIFT were removed from the SWIFTER design, with no major adverse impact on structural rigidity.

Figure 17 - SWIFTER test (L) and non-test (R) surface interior faces

Worst case scenario loading Factor of Safety (FoS) analyses were carried out by Tom Duncan, using Solidworks Finite Element Analysis package. The worst case scenario is based on a 2G pull up and 30 degree bank, simulating a mid-dive abort. With 550lbs of lift on the model, 175lbs of which were applied to the leading edge, 40lbs of drag, and the 2G inertial loading, all factors of safety were found to be well over the minimum target of 1.5. Based on operational experience with the SWIFT model, with which any change to the internal configuration of the model required unmounting it from the wing of the O-2A, laying it on a workbench, and removing all connectors to split the model in half, it was decided that a better solution was to add access panels to the non-test surface. These would allow the interior components to be examined and modified with the model still in situ, either on the wing of the O-2A, or in the test section of the KSWT. Four panels were added (Figure 18), two in a vertical orientation just aft of the leading edge, for access to the actuation system, and two further aft in a horizontal orientation, for access to pressure ports and other instrumentation. A thickened ridge was added to the non-test surface around each of the panel locations to allow the panels to sit flush with the surface, while still being securely held in place by retaining bolts.

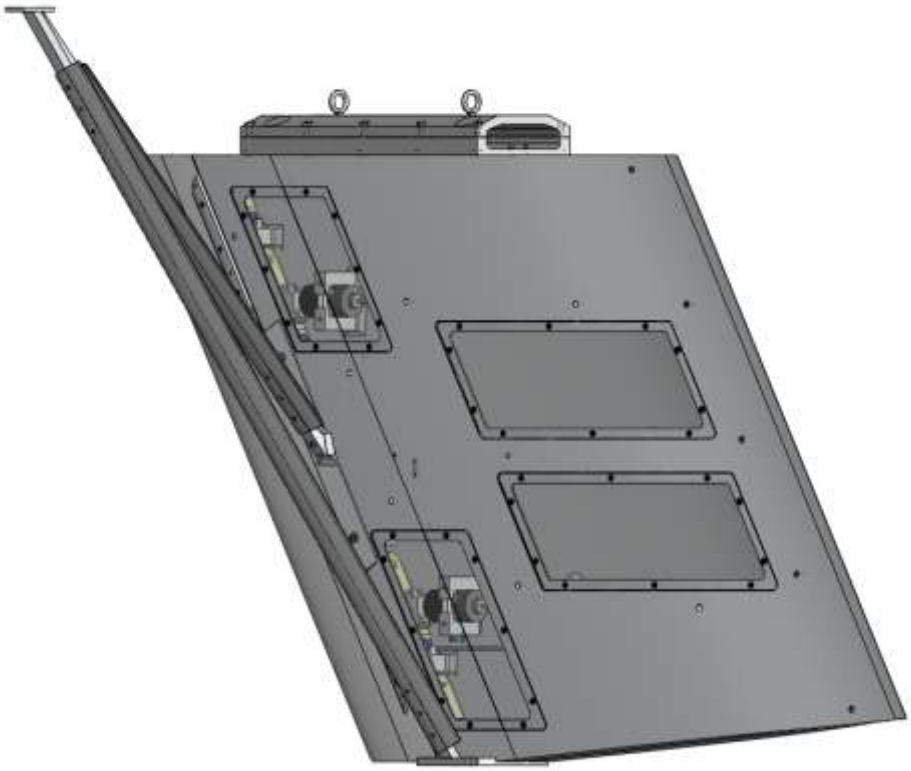

Figure 18 - SWIFTER non-test surface side showing access panels

When mounted to the outboard pylon of the O-2A, the model interfaces through a two-piece aluminum channel section (Figure 18, top) with two titanium eyebolts that connect into the mounting hooks of the pylon. On the SWIFT model, this channel was slotted to allow the angle of attack of the model, β, to be adjusted to suit the experiment being conducted. However, throughout the course of testing, the angle was never adjusted, and left at one degree toe out.

To simplify the design for SWIFTER, it was decided to remove the adjustment capability, and instead have a fixed β of four degrees toe out. This angle was chosen as the majority of tests are conducted in the vicinity of four degrees toe out, and setting the model into this range would reduce the sideslip angle that would be required to be flown by the aircraft. The five hole probe is mounted to the non-test surface on an L-section piece of aluminum supported by two stand offs. On SWIFT, a major time factor in mounting the model to the wing of the O-2A was the alignment of the five hole probe. The procedure involved marking chalklines on the floor of the hangar in line with the model chordline and the probe, measuring the angular offset, and adjusting the probe until it fell within +/-0.1 degrees of the chordline. This could take over two hours to complete.

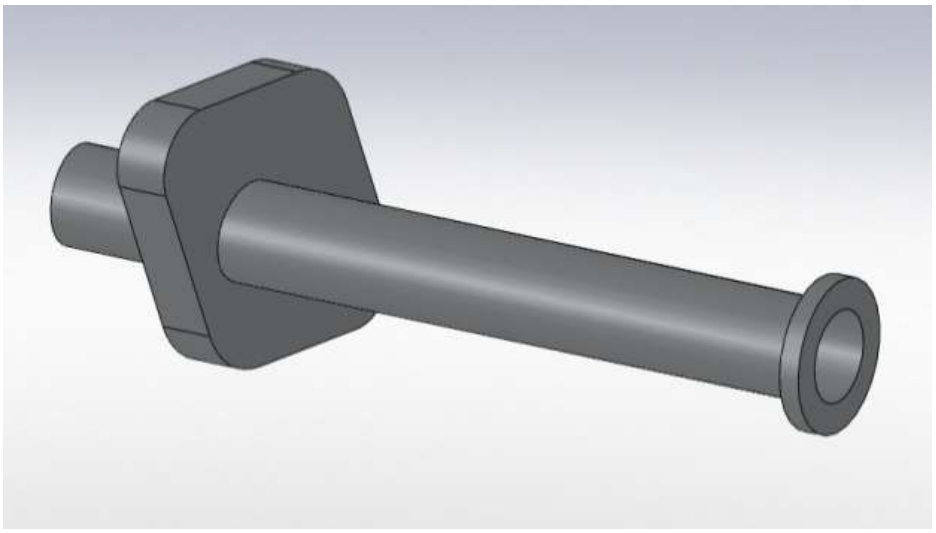

Figure 19 – New five hole probe mount standoff

To attempt to improve the mounting procedure, new standoffs were designed with the curvature of the non-test surface machined into their base (Figure 19). The aim of this was to have a self-aligning system that, after verification, would allow the mount to be installed and be sure of correct positioning. As with SWIFT, the test and non-test surfaces, as well as one of the two leading edges, are outfitted with two rows of pressure ports in order to validate the computational pressure coefficients throughout the target β range.

The primary difference between SWIFTER and SWIFT is the leading edge actuation system. Unlike SWIFT, where the leading edge was directly bolted to the test and non-test surfaces for maximum rigidity, in order to allow the creation of step and gap excrescences, the leading edge on SWIFTER is supported by actuator lead screws and guide shafts mounted to rail guides on pylons from the main body of the model. Due to this less rigid mounting solution, modifications had to be made to the test and non-test surfaces in order to minimize relative displacement between the test surface forward face, and leading edge aft face. Another factor considered was the uniformity of relative displacement across the entire span of the model, as if this could not be minimized, the excrescences created could not rightly be called two-dimensional. After several iterations of finite element analysis, a final configuration was reached which gave uniformity of relative displacement across the center span of the model of less than 25μm, which was deemed sufficient, as it matched the accuracy to which Northrop set their step excrescences in the SETS experiments. This configuration resulted in thickening the first eight inches of the test surface to 0.5 inches, with the central 11

inches thickened further to 1.0 inches (Figure 20). The matching section of the non-test surface was also thickened similarly.

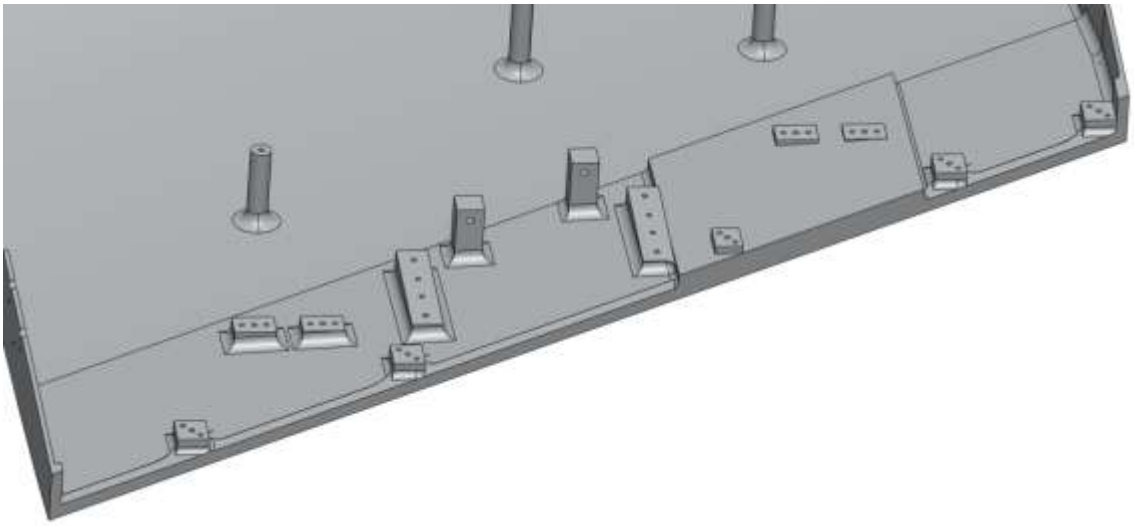

Figure 20 - SWIFTER test surface thickened sections

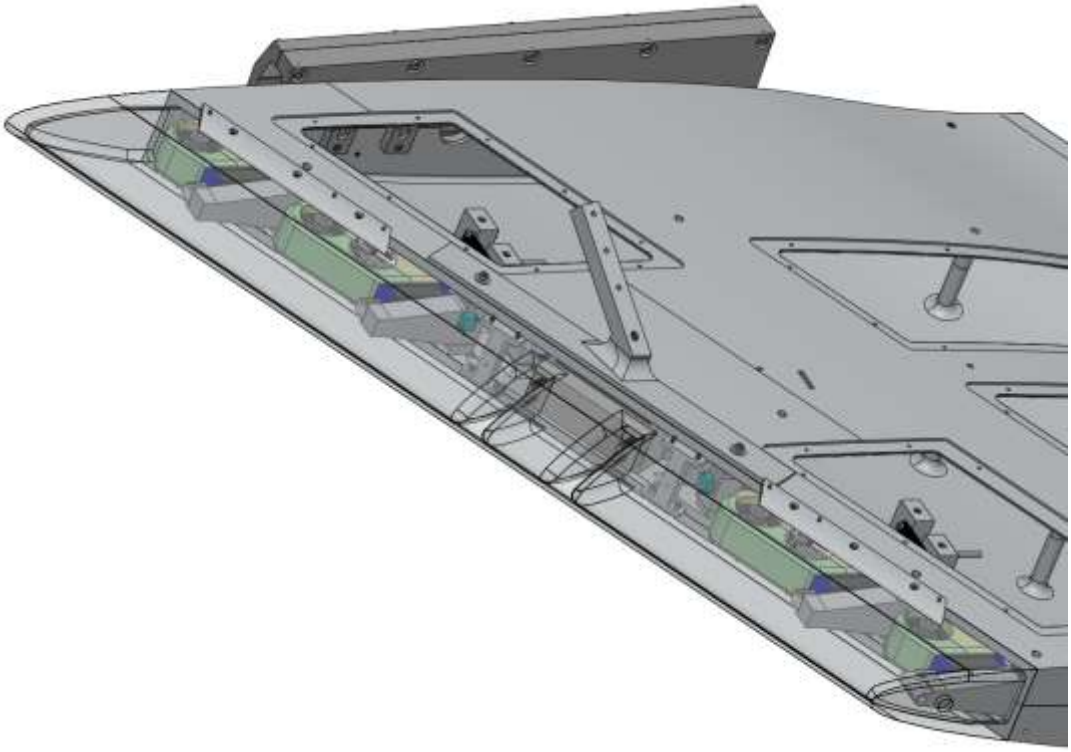

Figure 21 - SWIFTER leading edge cutaway showing actuation system

The leading edge actuation system (Figure 21) consists of motion hardware, guide and restraining hardware, and position feedback hardware which work in conjunction to smoothly move and restrain the leading edge in whatever configuration is desired by the test operator. The motion hardware consists of four Anaheim Automation 23A stepper motors (Figure 22), two for step actuation, and two for gap, with a linear travel per step of 6.4μm. Each motor can drive 100lbs force, more than enough to move the leading edge in operational conditions, and when not in motion, cannot be moved from its

stopped position, unless an extreme load occurs which strips the threads of the hardened steel lead screw. The leading edge step actuator mounts are connected to Thomson linear rail guides on pylons from the main body of the model. These support any non-axial loading on the lead screws of the gap actuators. Lateral loading on the step actuator lead screws are supported by four solid shafts running through bearing blocks in parallel with the actuator mounts. These shafts also minimize any looseness in the system that could cause the actuators to bind.

Figure 22 - Anaheim Automation 23A stepper motor

Figure 23 - AEC Magnetics electromagnet

Lateral and axial loading of the leading edge is also supported by an AEC Magnetics electromagnet (Figure 23), rated at 1500lbs force, mounted midspan in the model body. It connects to a one inch thick low carbon steel block in the leading edge. As only two thirds of the magnet face is in contact at any time, a proportional axial restraining force of 1000lbs is applied to the leading edge. As the shearing load is rated at 25% of the axial force, 250lbs force supports lateral loading of the leading edge.

Figure 24 - Unimeasure ZX-PA displacement sensor

Position feedback in both the gap and step directions of motion is provided by three Unimeasure ZX-PA "stringpot" displacement sensors (Figure 24). These potentiometer sensors have a measurement range of 38.1mm, and a repeatability of +/-0.03%, in this case, within 11.4μm. Position is measured via a nylon jacketed wire cable, which allows the sensors to remain connected even when the sensor mounting point and cable connection point are not aligned. The position can then be calculated through relations from both the gap and step sensors. One of these sensors is mounted in the gap direction, and two are mounted in the step direction, one towards the tip, the other towards the root. This allows the uniformity of the step excrescence to be monitored, and motion stopped if the actuators appear to be driving the leading edge out of alignment.

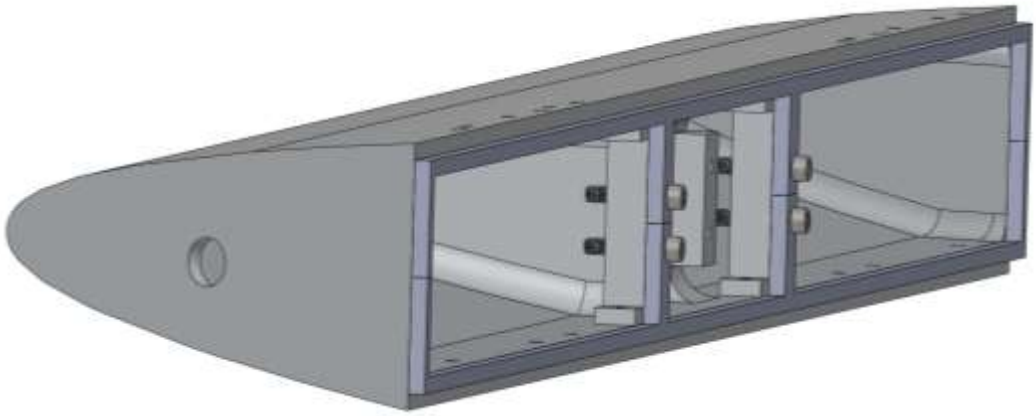

Figure 25 - Leading edge gap inserts

If a non-zero gap configuration is desired, gap inserts cut from sheet aluminum of a known thickness can be bolted into position on the aft face of the leading edge (Figure 25). To allow these inserts to be installed without removing the leading edge completely from the model, they will be split in half along the span of the model, allowing them to be inserted from the left and right sides of the model. As a perfect seal between the leading edge and the main body of the model is required to prevent any leakage into the test surface boundary layer, a compressible polytetrafluoroethylene (PTFE) gasket tape will be applied to the aft face of the leading edge, and Kapton tape to the forward face of the test and non-test surfaces. After preliminary smoke leakage tests, it was found that tape of thickness 0.5mm provided adequate sealing.

Flight Research Laboratory (FRL)

The FRL operates a 1968 Cessna O-2A– a high wing, twin engine aircraft with centerline thrust and twin tailbooms (Figure 26). This aircraft is a militarized version of the Cessna 337, with modifications including four wing-mounted pylons, reinforced wing spars, enlarged observation windows for both pilot and copilot, and a rack system in the aft of the cabin, originally for radio equipment. Through a large library of aircraft performance and safety analysis data, and a history of operation over the past few years with the FRL in the SWIFT test program, the aircraft has been found to be well suited to the role of experimental research platform. Flight crew for experimental operations consists of a pilot in the front left seat, a copilot/safety observer in the front right seat, and a flight test engineer (FTE) in the rear right seat. The pilot flies the aircraft relying on target point data provided by the FTE during all test phases, while the copilot maintains situational awareness of the surrounding airspace, as well as assisting in test operation and data recording when required. The FTE is the primary test operator, calling all configuration changes, monitoring the test parameters, and commencing and terminating test phases. Ground crew consists of two personnel responsible for preflight documentation, final exterior inspections, and communications with the flight crew while airborne by way of a ground radio operations station at the FRL, with the callsign "Aggie Base".

Figure 26 - Cessna O-2A

Test operations are conducted in two non-congested airspaces in the vicinity of Easterwood Airport (KCLL). The test area for an operation is chosen based on weather and sun location considerations. All flights are tracked by flight following, and confirmation of clear airspace is made before any test maneuver is begun. Previous experiments with the O-2A have required the flight profile to consist of a climb to an altitude of 10,500ft, followed by a cold soaking period of 20 minutes. With the model cooled to ambient temperature, the aircraft was then placed in a dive at 175KIAS to

achieve a target Reynolds number of $7.5x10^6$. The angle of attack of the model, β, is then held at the point specified by the FTE. As the aircraft descended, the ambient temperature increased, and the model would warm up. IR thermography was used to visualize the transition front. The dive would then be terminated at 3,000ft for safety reasons.

With the new SWIFTER program, however, the range of target Reynolds numbers is wider, as the aim is to extend the dataset from the Northrop SETS experiments, which only go as high as $4x10^6$. Therefore, not all flight operations will require a dive to reach the target Reynolds number, and it can be achieved in level flight. This has the benefit of increasing the time aloft, and the amount of data that can be collected. In addition, the range of weather conditions in which the tests can be conducted is expanded, as if there is an overcast cloud deck that would normally prevent operations due to moisture concerns, the test can be carried out below that altitude.

FRL Instrumentation

To measure flight data, the O-2A is outfitted with an Aeroprobe conical tip five hole probe mounted to the non-test side of the model (Figure 27), and a Resistive Temperature Detector (RTD) mounted on the port wing. The five hole probe is capable of measuring pitch, yaw, static pressure and dynamic pressure. The ports are connected to four Honeywell FP2000 pressure transducers located within the model. Combined with the temperature, this provides a record of altitude, true airspeed, Mach number, and Reynolds number. To record freestream turbulence levels, a sting mount with a NACA 0015 airfoil is mounted on the starboard wing. It holds an array of four hotwires and allows turbulence levels to be measured, correlated, and acoustic disturbances removed for a more accurate reading.

Figure 27 - Five hole probe

A hotfilm array, with associated Preston tube shear stress measurement device, static pressure port, and thermocouple for calibration, can be applied to the test surface of the model if higher accuracy transition measurements are required. Two AA Systems AN-1003 anemometers can be mounted on the rack to receive both the hotwire and hotfilm data. The information is processed through a pair of National Instruments DAQ boards – a USB-6259, with 16 differential analog input channels, and a sample rate of up to 1.25Mhz, and a USB-6255 for 16-bit analog to digital conversion, and fed to the FTE's flight laptop, running a custom Labview program.

Figure 28 - Yoke-mounted pilot display

A yoke-mounted display (Figure 28) provides real-time updates on target Reynolds number and β, as well as their rate of change, to the pilot, allowing them to maintain values within tight bounds. The display is also used to review the atmospheric temperature profile with the FTE before commencing a dive, in order to better anticipate any possible temperature inversions or turbulence. All system 115VAC power is provided through an 1100W inverter connected to the aircraft battery. Power can be killed by either the FTE or the pilot in the event of an emergency.

To visualize transition on the test surface of the model, a FLIR Systems SC8200 Infrared camera is used. This uses an Iridium Antimonide (InSb) detector, and operates in the 3-5μm (mid-band) spectral range. It is designed to operate in a temperature range of -40^{o}C to 50^{o}C, and to a maximum altitude of 40,000ft. It has a resolution of 1024 x 1024 pixels, and can sample at up to 132Hz, but for normal operations, a maximum of 30Hz is used to minimize bandwidth issues over the Gigabit Ethernet connection to the flight laptop. The camera is operated by FLIR's ExaminIR software, providing both recording and real-time display of the thermal image. This is constantly monitored during test procedures by the FTE, who can then use it to aid in making calls on when to switch to the next test points. The camera is mounted to the instrumentation rack in the aft of the cockpit of the O-2A, and views the model through an open section in the left side passenger window, as the Plexiglass cabin window would prevent transmission of the 3-5μm spectral range.

The FRL has two lenses for use with the camera – a 17mm focal length, and a 50mm focal length. The 17mm lens has a 56.9^{o} field of view (Figure 29), which allows for an overall view of the model. The 50mm lens has a 20.9^{o} field of view which allows for a more in-depth view of regions of interest across the test surface of the model. Ground tests with a 4.5mm x 1mm striped pattern (Figure 30) show that it is theoretically possible for the SC8200, fitted with the 50mm lens, to resolve crossflow instabilities on the test surface of the model, a valuable research asset, to which the FRL has not had access to this point.

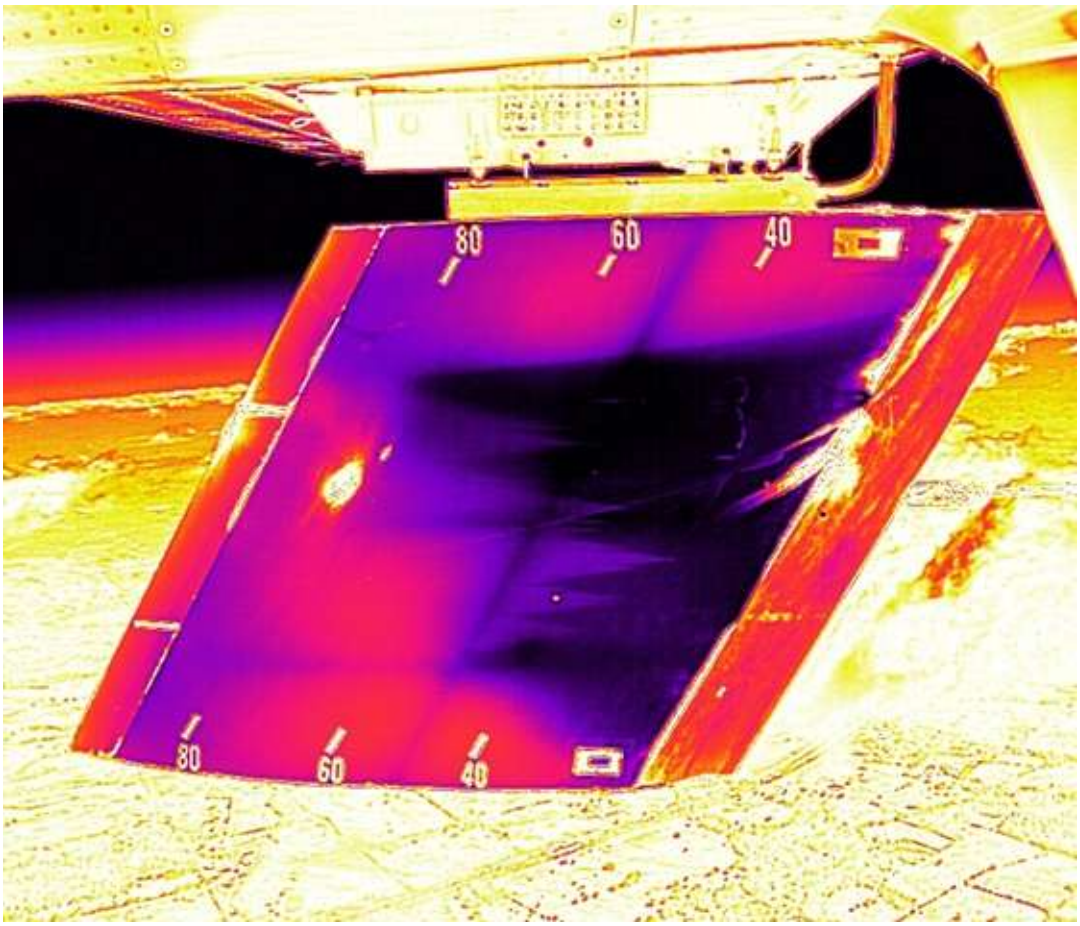

Figure 29 - SC8000 IR image of SWIFT model (17mm lens)

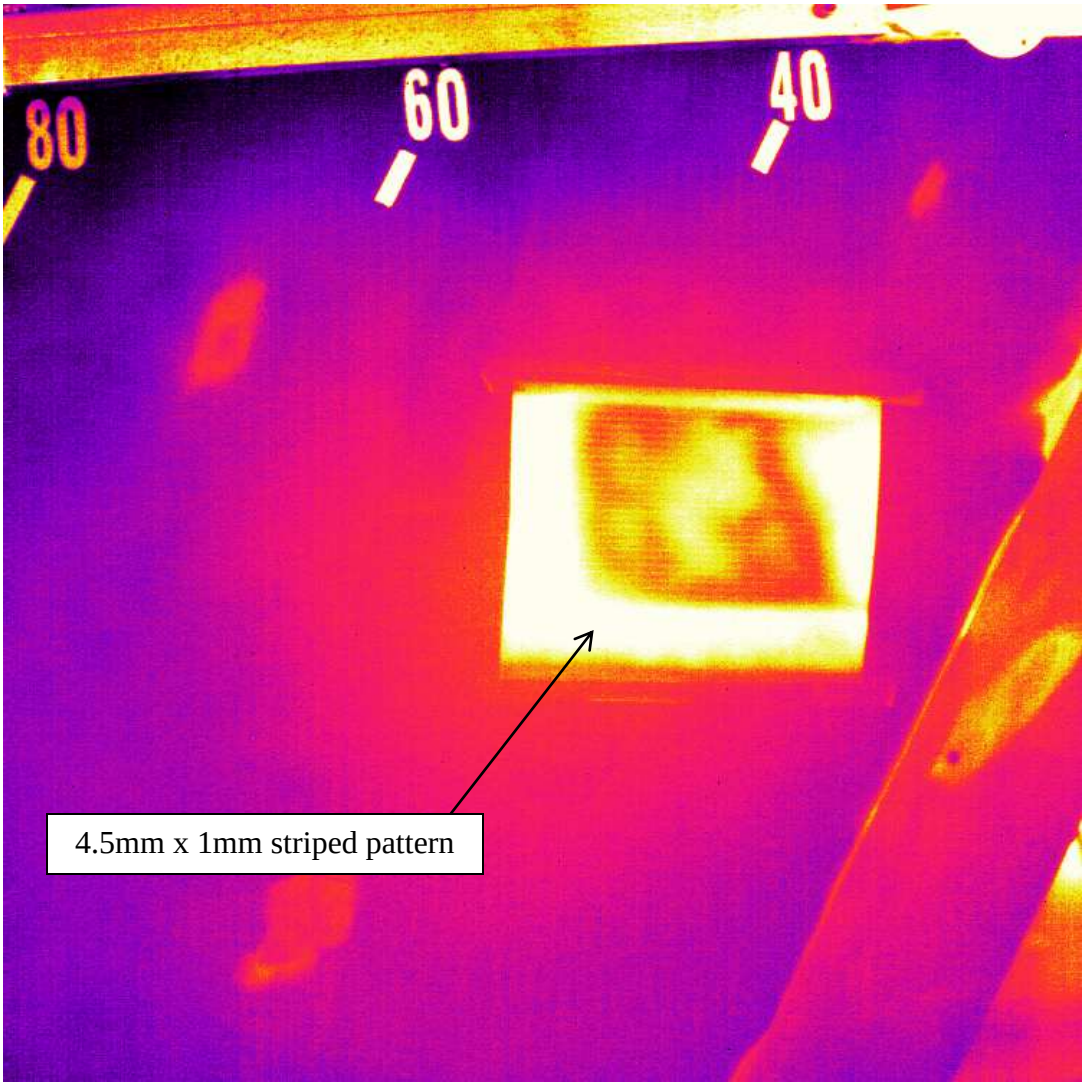

Figure 30 - Resolution of representative crossflow pattern with 50mm lens

Klebanoff-Saric Wind Tunnel (KSWT)

The KSWT (Figure 31) is a closed-loop, low-speed tunnel, with extremely low disturbance levels. It is capable of speeds up to 31m/s, with an accuracy of +/-0.1m/s of the desired speed. The fan (Figure 32) is an adjustable pitch design, with nine blades, and is located downstream of the test section, on the return leg. Power is provided by an external 150hp DC variable current electric motor, mounted in an acoustically insulated enclosure below the fan housing, by way of a belt drive. Maximum RPM of the system is 1300, controllable to +/-1RPM. The test section (Figure 33) has a cross section area of 1.4m x 1.4m (4.5ft x 4.5ft) at the entrance, and 1.41m x 1.4m (4.64ft x 4.5ft) at the exit. This is due to the floor sloping downwards slightly to account for boundary layer growth on the tunnel walls. The section is supported on four isolated pedestals, with a Fabreeka Precision-Aire PAL 21 pneumatic isolator mounted to each, to minimize the transmission of vibrations from external influences. It is also not rigidly connected to the contraction cone or diffuser.

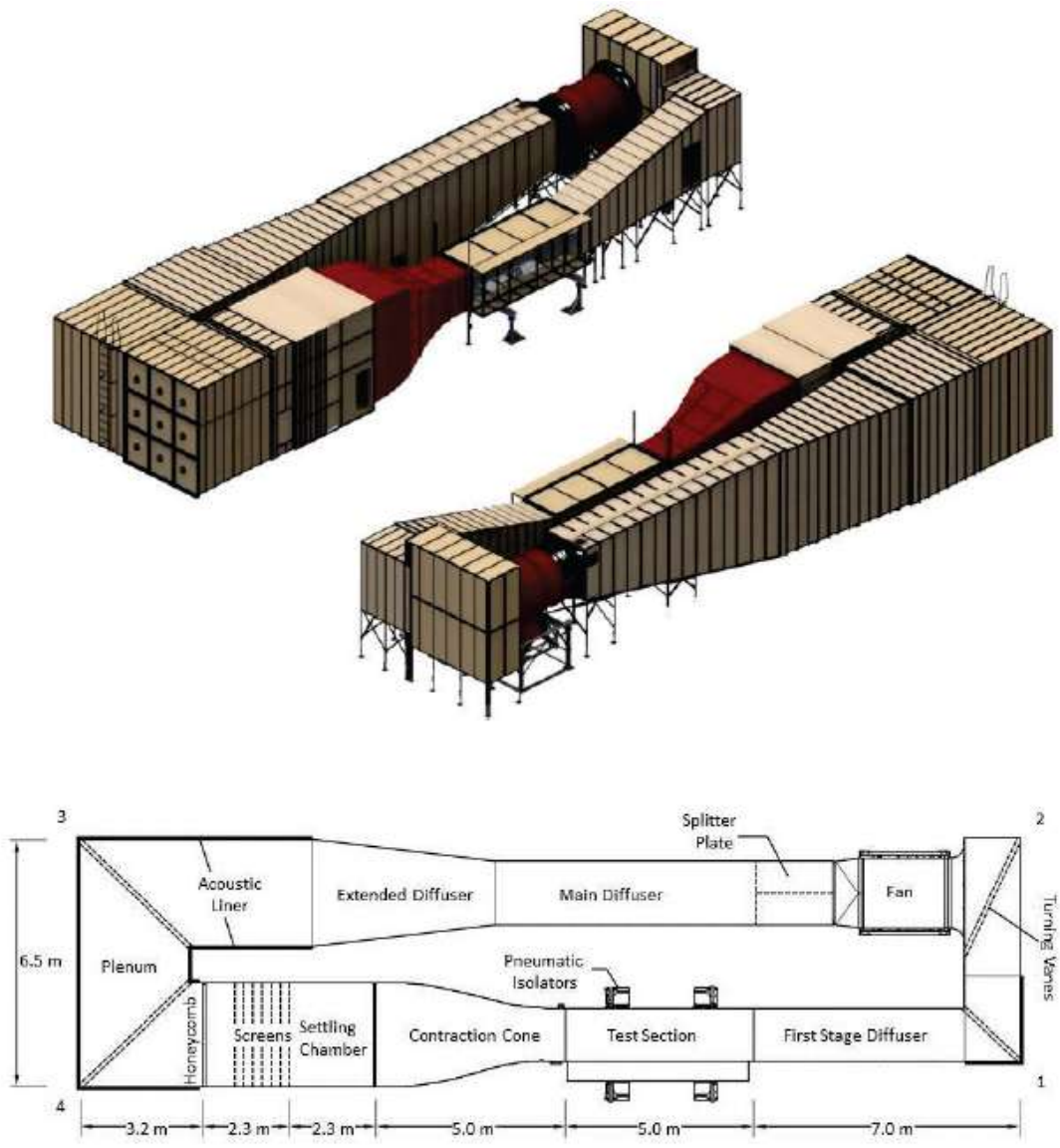

Figure 31 - Perspective & plan views of the KSWT

Figure 32 - KSWT fan in situ

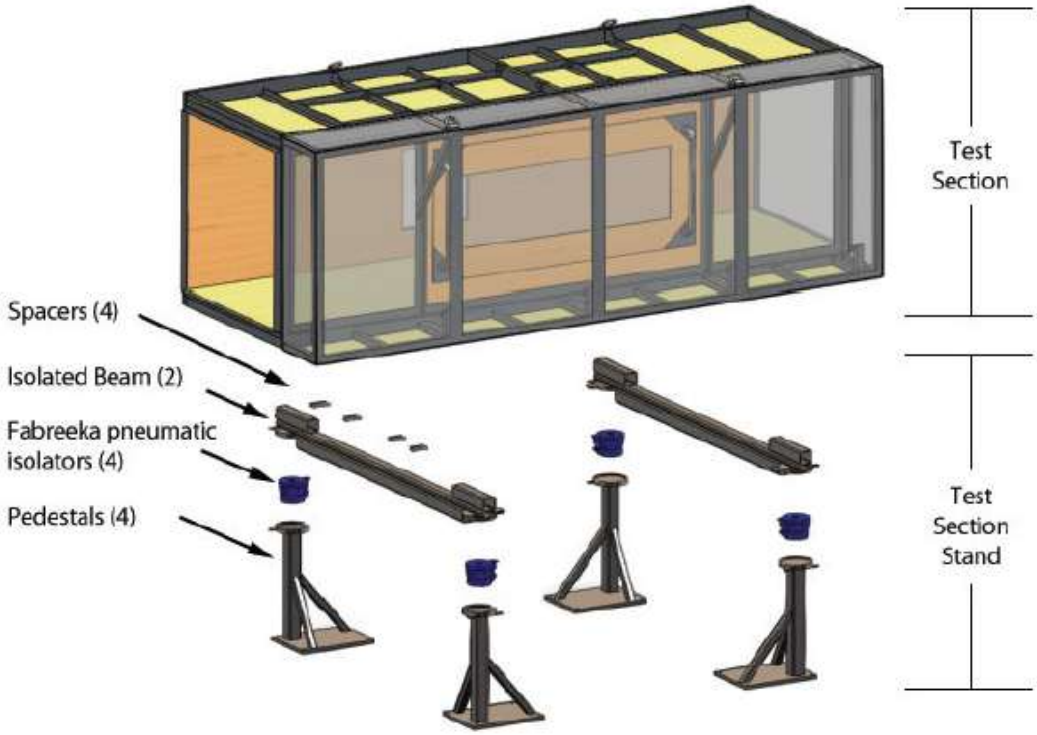

Figure 33 - KSWT test section and supports

The test section is removable by crane for model installation, preparation, or removal. Two test sections are available for use to minimize downtime during configuration changes. One is primarily used for swept wing testing, while the other is used for flat plate research. An interchangeable panel is mounted in the center of the test section, with the option of mounting a viewing/IR window or a hot wire traverse mechanism. To minimize disturbances in the tunnel, a variety of measures have been taken. In the main and extended diffusers, flow separation due to large angles was reduced by the addition of two screens and splitter plates, which also helps reduce large scale turbulence from the fan.

The plenum section is coated with two kinds of acoustic panel – broadband (50-5000Hz) damping plates, and 500Hz+ acoustic foam. These help to minimize the frequency band (50-400Hz) in which many of the tunnels instabilities exist. These treatments are also present in the first corner, to minimize noise propagation upstream. Turning vanes located at the all four corners aid in reducing overall background noise levels. A honeycomb mesh and seven wire screens are also included downstream of the fourth corner to reduce turbulence levers, and increase flow uniformity. Downstream of the screens, a 2.2m (7.2ft) settling chamber allows viscous dissipation to reduce disturbance intensity further. This then leads to the contraction cone, with a 5.33:1 ratio, and zero slope and curvature ends to minimize differing turbulence intensities, and to reduce the risk of a separation bubble forming, causing pressure fluctuations.

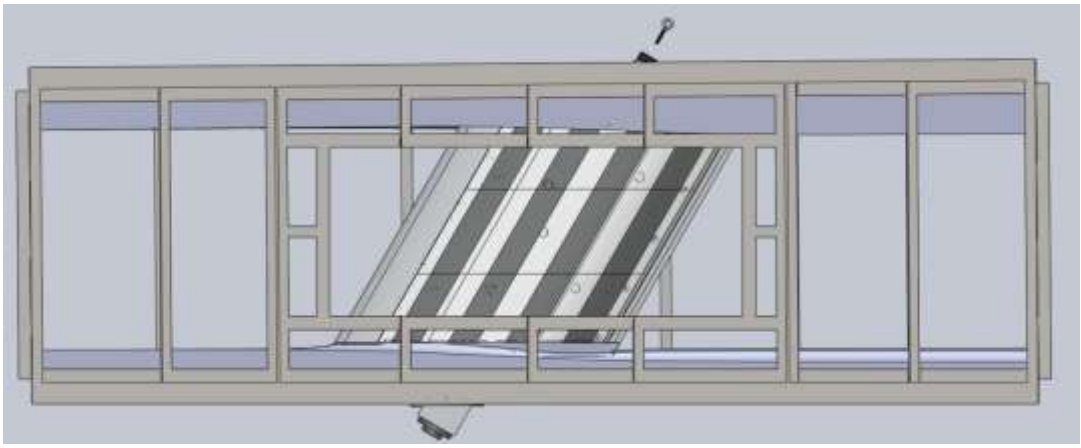

Figure 34 - SWIFTER mounted in KSWT test section

As SWIFTER was designed to be mounted on the FRL's Cessna O-2, it is optimally viewed from the right side, facing downstream. However, the KSWT test section is designed for the test surface to be on the left side, facing downstream (Figure 34). This necessitated the mounting of the model inverted from its normal orientation, and with the sweep now sloping aft from the lowest forward point to the highest. Precautions will have to be taken during tunnel operations to avoid dust and debris buildup on the exposed leading edge. In addition, when working around the model, tunnel personnel will have to be very conscious of the risk of dropped tools and equipment. The mounting hardware allows for adjustment of the angle of attack of the model in increments of 0.2 degrees.

KSWT Instrumentation

Freestream data is measured in the tunnel with a pitot static tube located nine inches downstream of the test section entrance, and a RTD located just below it. The pitot static tube is connected to Baratron absolute and differential pressure transducers. These measurements combine to provide freestream velocity measurements accurate to +/-0.1m/s. These data, along with test data, are recorded with a trio of National Instruments USB-6211 DAQ boards. This is integrated with the tunnel control software, which is controlled by a terminal interface. The tunnel can be set to maintain constant velocity, Reynolds number, or fan RPM. In addition to the directly relevant test parameters, the motor and fan temperatures are monitored, along with the pressure values for the test section pneumatic isolation system in order to ensure the normal operation of the tunnel. Warnings are shown to the tunnel operator when out of range values occur. The primary method for determining boundary layer transition location on the test surface of SWIFTER in the KSWT will be infrared thermography with the FLIR Systems SC8000 camera, as when mounted on the O-2A.

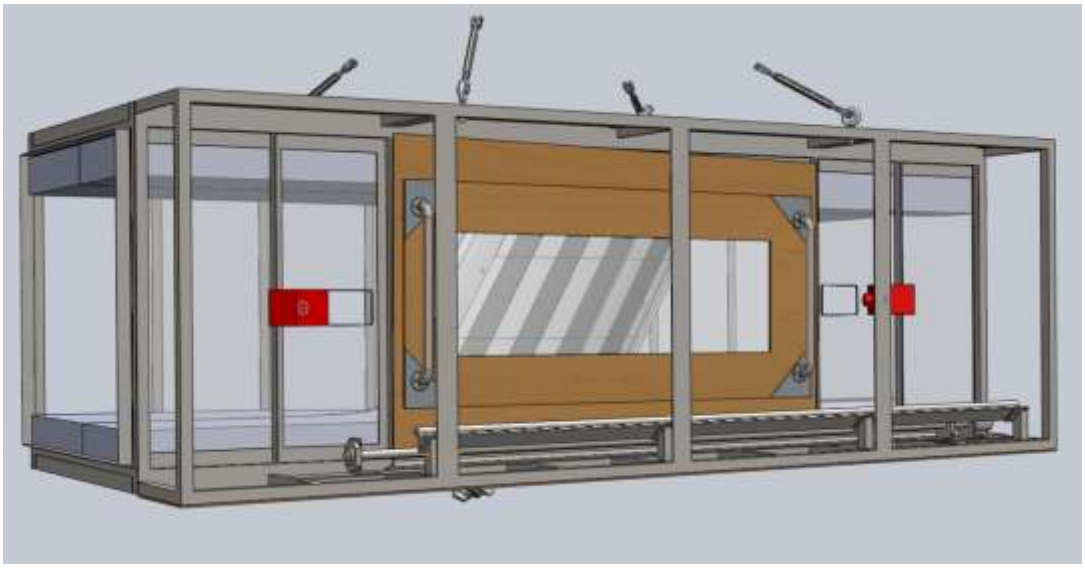

Figure 35 - Upstream and downstream camera positions

The camera will be mounted to the metal frame of the traverse box on the outside of the test section. Several positions, to be finalized, will be utilized to give the best range of views of the test surface, and particular regions of interest that arise. These potentially include upstream and downstream positions (Figure 35), with ports cut through the Plexiglass panels to allow transmission of the 3-5μm spectral range. It should be noted that only one of these ports should be open at any one time to prevent circulation through the traverse pressure box, and the flow over the model being affected. A new viewing panel with several IR transparent windows along its length will allow more in-depth analysis across the test surface, using the 17mm lens.

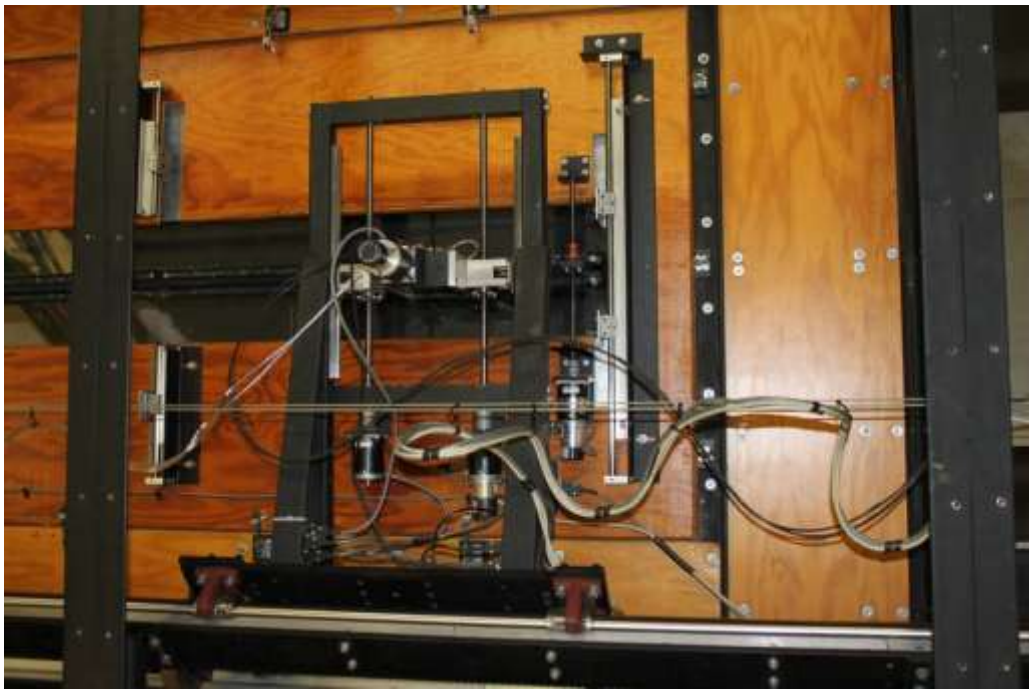

Figure 36 - Hotwire traverse system

If a detailed study of the boundary layer profiles on the test surface is required, the hotwire anemometry traverse system (Figure 36) can be used. The system consists of a high precision three-axis traverse with two probes on a sting mount – one for freestream readings, and one for the boundary layer. The bulk of the mechanism is outside the test section, within the pressure box. A single lead screw and two guide rails control the streamwise motion of the traverse frame. Mounted to this, two lead screws control the spanwise motion of the hotwire sting mount. Finally, a single lead screw controls the wall normal motion of the sting. All of the lead screws are driven by Compumotor microstepping motors, while position is given by Renco encoders. Minimum steps are 11.9μm in the streamwise direction, 1.27μm spanwise, and 0.64μm wall normal.

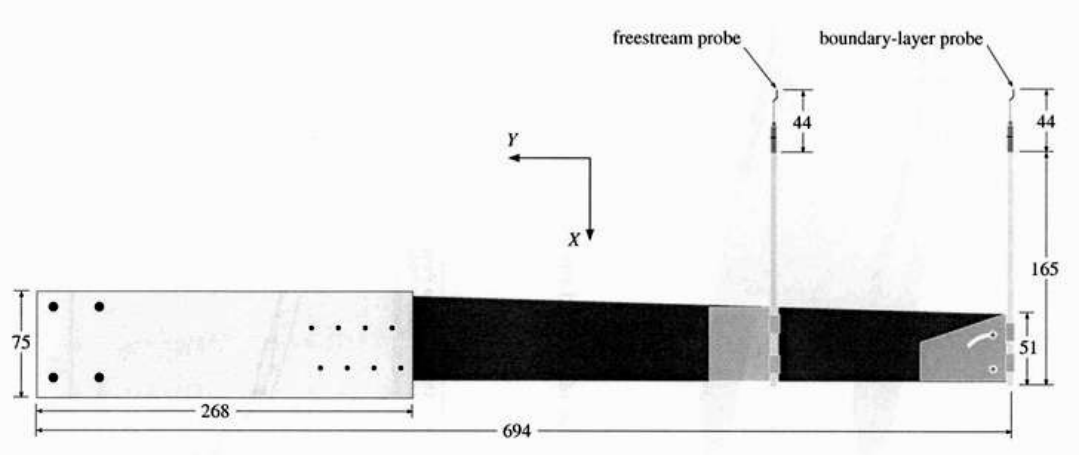

Figure 37 - Hotwire sting mount (top-down view) (White, 2000)

The sting mount (Figure 37) is the only part of the system that extends into the test section proper. It consists of a thin tapered airfoil shape with two hotwire probe mounts extending upstream. It enters the test section through a streamwise zippered slot in the Plexiglass traverse window. This zipper keeps the opening closed to either side of the sting mount to minimize venting of the test section. The slot translates with the spanwise motion of the system. The sting mount generally completes a boundary layer scan in an automated sequence during a test run, based on parameters input by the tunnel operator. It can also be positioned by direct command input, if desired.

CHAPTER III

THEORY

Flow Over Step and Gap Excrescences

For an aft-facing sharp step, the flow detaches immediately at the corner (Figure 38). The separated shear layer then curves downwards and reattaches to the surface. Below the shear layer is a recirculating vortical flow region with maximum backflow velocities of over 20% of freestream velocity (Castro & Haque, 1987). Reattachment can be unsteady, with the point at which the flow reattaches changing as a result of momentary flow reversal in the shear layer, causing the separation bubble to momentarily collapse (Driver, 1987). Whether the flow reattaches in a laminar or turbulent manner determines whether or not the overall flow immediately transitions to turbulence aft of the step. Forward-facing steps (Figure 39) develop a separated recirculation vortical flow region at the forward face of the step. For all but very low Reynolds number flows, a second separation region also develops on the top surface of the step immediately aft of the forward edge. For configurations with a forward-facing step leading an aft-facing step, as in the work of Fage, interaction between the two separated regions cannot be ruled out.

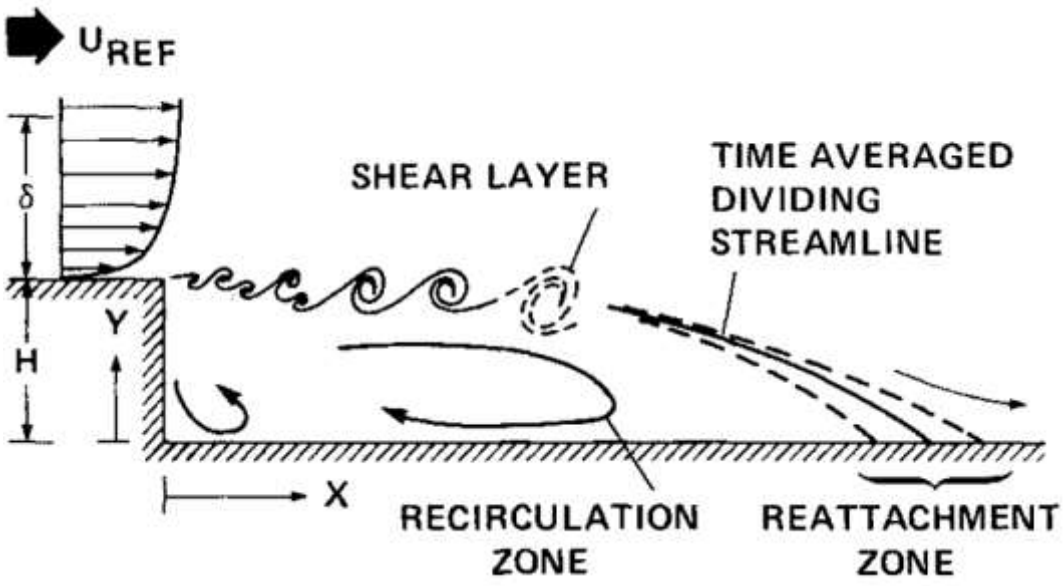

Figure 38 - Flow over aft-facing step geometry (Driver, 1987)

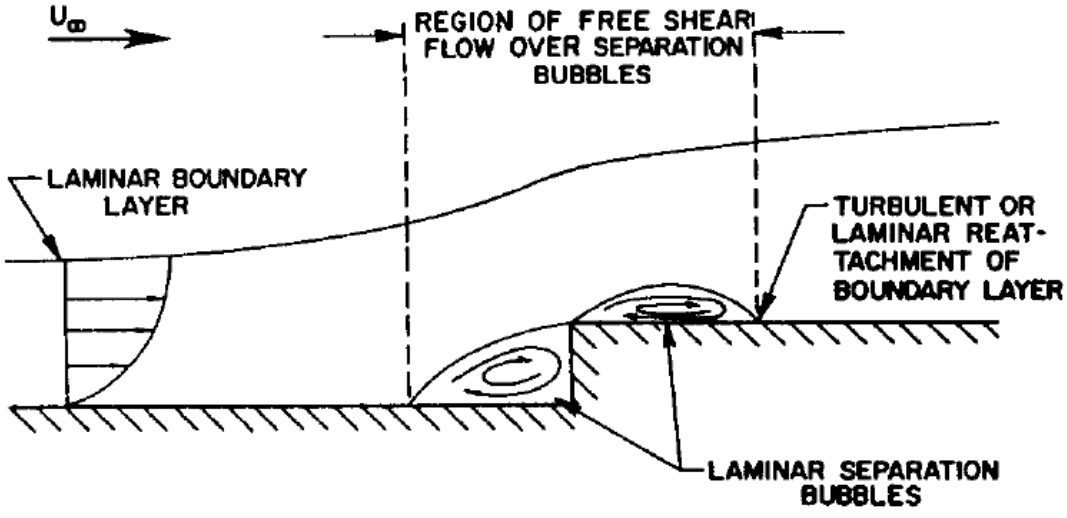

Figure 39 - Flow over forward-facing step geometry (Obara & Holmes, 1985)

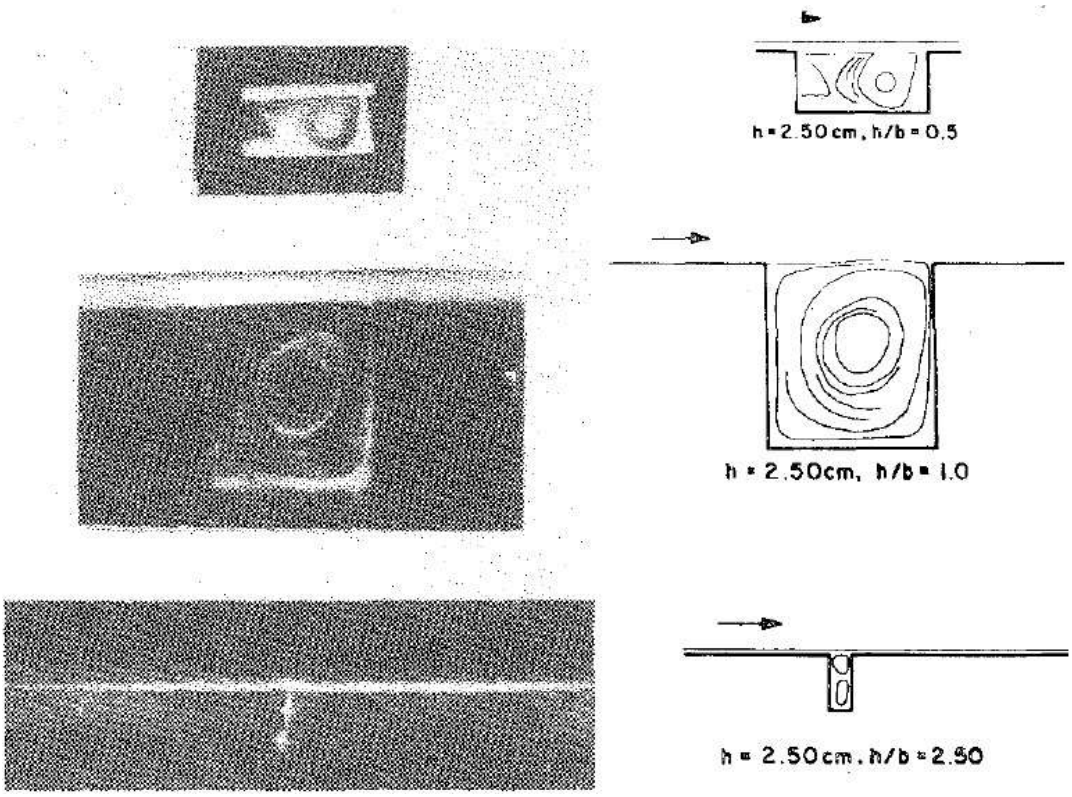

Figure 40 - Smoke visualization and schematics of gap flow (Sinha et al., 1982)

Flow over small gaps (Figure 40) has much less of an influence on transition to turbulence than flow over steps, either forward-facing or aft-facing. This can be attributed to the more self-contained nature of the separated flow region. For gaps with height to width ratios of around 1:1, a single, centered vortex structure develops, whereas for a gap with a deeper ratio of 2.5:1, two stacked vortices develop (Sinha et al., 1982).

Flow Instabilities

Although the precise mechanism for breakdown to turbulence of the flow over step and gap excrescences is not yet well understood, a brief discussion of the primary instabilities relevant to this application is worthwhile, so that any phenomena observed may be seen in the context of what is known for flow over swept wing airfoils in general. The relevant instabilities are Tollmein-Schlichting (T-S) waves, crossflow vortices, and the free shear layer instability.

Tollmein-Schlichting (T-S) waves are a streamwise, two-dimensional viscous instability, and dominate the transition process of most two-dimensional boundary layers, such as unswept wings and flat plates. They are sensitive to freestream conditions, sound, and two-dimensional roughness (Saric, 1998). However, they are insensitive to three-dimensional roughness. Their initial amplitudes come from the freestream, and they are slow growing. Positive pressure gradients stabilize the waves well, and weak wall suction can also be used for control. T-S waves are relevant to this investigation of step and gap excrescences as a wide variety of two-dimensional excrescences will be tested. Even though they are stabilized by the overall positive pressure gradient of the airfoil, larger magnitude excrescence configurations may induce their growth due their sensitivity to two-dimensional roughness, and due to local generation of adverse pressure gradients.

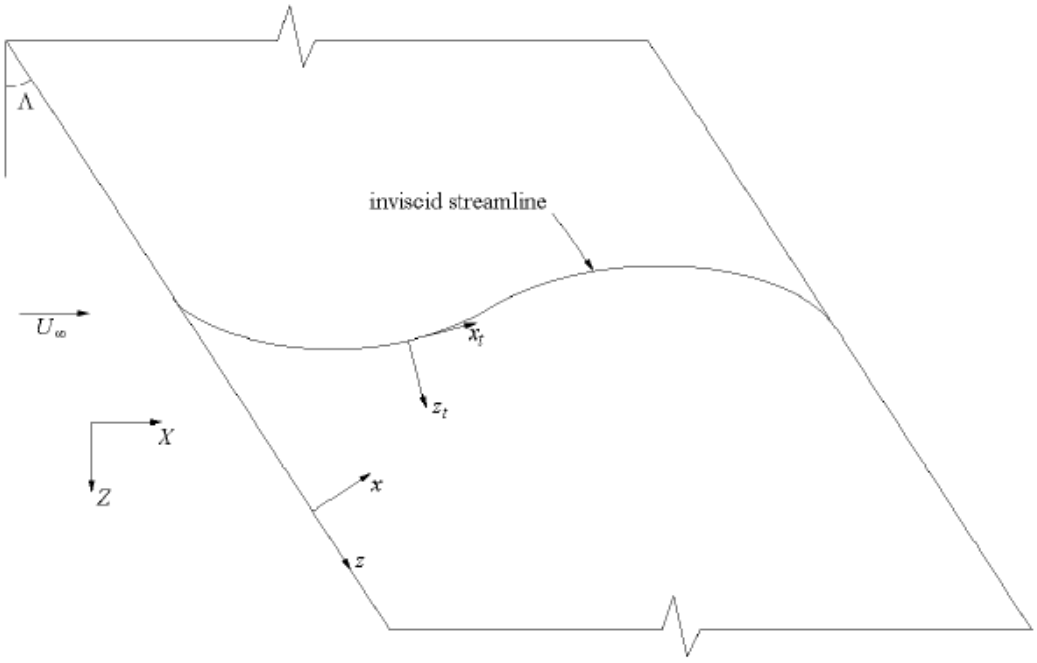

Figure 41 - Streamline deflection on a swept wing

Crossflow vortices come from the existence of a pressure gradient on the surface of a swept wing, which deflects the streamlines over the airfoil inboard, on the suction side, as far aft as the pressure minimum, at which point the streamlines deflect outboard (Figure 41). Within the boundary layer, this centrifugal acceleration is not balanced by the pressure gradient, and the fluid velocity reduces. This imbalance creates a secondary flow within the boundary layer orthogonal to the inviscid streamlines. This means that the boundary layer velocity profile (Figure 42) contains an inflection point, subject to an inflectional instability – streamwise co-rotating vortices that cause breakdown to turbulence by way of mean flow distortion, and inflectional instabilities. The fact that,

unlike T-S waves, crossflow is destabilized by a positive pressure gradient makes it a complicated problem to solve.

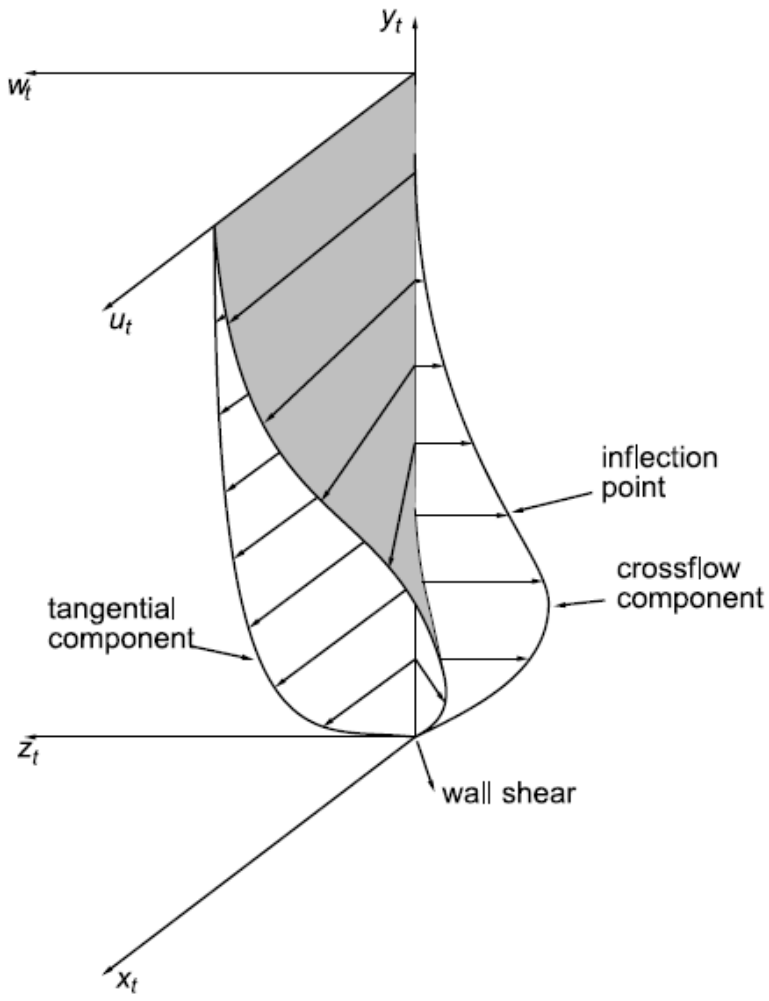

Figure 42 - Swept wing boundary layer profile (Saric, 2010)

The crossflow instability is sensitive to freestream turbulence and three-dimensional roughness. In a low turbulence environment, such as flight, stationary vortices are dominant, whereas in a higher turbulence environment, greater than 0.15% intensity (Deyhle & Bippes, 1996), travelling crossflow dominates. Surface roughness levels have also been found to affect which form is present (White, 2000). As the test airfoil has a positive pressure gradient, the crossflow instability is expected to be a factor in the transition to turbulence, despite showing insensitivity to two-dimensional roughness at low amplitudes (Radetsky et al., 1999).

The inviscid free shear layer instability can develop along the shear layer separating the flow over the separation bubble from the vortical structures within it. It comes as a result of the inflection in the velocity profile caused by the abrupt change in the momentum of the fluid in the wake of the surface excrescence. High momentum fluid above the shear layer and low momentum fluid below mix, by way of a Kelvin-Helmholtz mechanism, and grow the shear layer thickness, as can be seen in Figure 38. The fluid entrained in the shear layer creates a positive pressure gradient, causing it to curve down towards the surface, and impinge at the reattachment point. Vortex shedding occurs at this point and the shed vortices can contribute to transition to turbulence downstream of the separation bubble, if turbulence does not immediately occur when a new boundary layer forms at reattachment.

CHAPTER IV

ACTUATION CONTROL SYSTEM

As mentioned in Chapter II, the leading edge of the model can be actuated to create step and gap excrescences by use of a combination of motion, restraining, and feedback hardware. This set of hardware must be controlled as a whole, by way of a control system that allows the operator to enter the desired parameters of step height, or gap width, without regard to the minutiae of the individual processes that occur to allow their goal to be accomplished. For this to be achieved, the operation of each hardware component in the system, how it can be controlled from the Labview software, and how that software can tie all of the various inputs and outputs together must be discussed.

For the development of this proposed SWIFTER actuation system, two National Instruments data acquisition (DAQ) boards were used to interface between the actuation hardware and Labview software. A USB-6211 board provided the high-speed digital output channels, along with the analog inputs, while a USB-6501 board provided extra digital channels. For the actual operational control of SWIFTER, a National Instruments X-Series USB-6341 board consolidated all the channels onto one board, while also providing higher resolution and better hardware timing options.

Linear Actuators

The linear actuators are stepper type electric motors. They consist of a series of eight stators on the inside of the casing, spaced at 45^{o} intervals, each with five teeth, spaced at 7.2^{o} intervals, wired in two alternating phases. The rotor, attached to the drive nut in the center, has two sets of 50 poles, North and South, around its circumference, and offset from each other by a half pole-width. Rotating the actuator through one step is achieved by switching power and current direction between the two phases of the windings, gradually incrementing the position of the rotor, as seen in Figure 43. This allows 200 1.8^{o} step increments in rotation, translating by the pitch of the lead screw to 6.35μm axial motion per full step. Micro-stepping, or dividing the step angle into smaller angles, can be produced by supplying proportional current to the windings by sine and cosine functions.

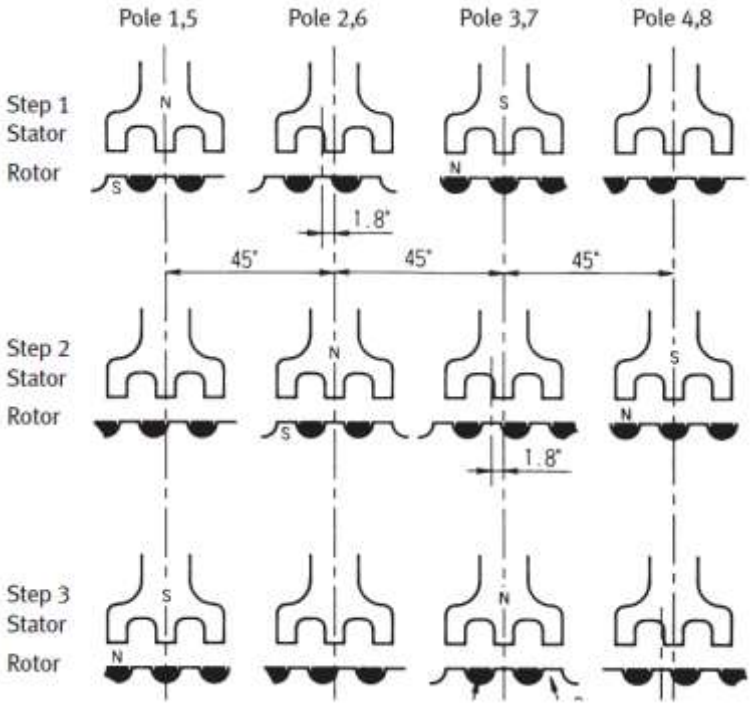

Figure 43 - Phase excitation of a stepper motor (Shinano.com)

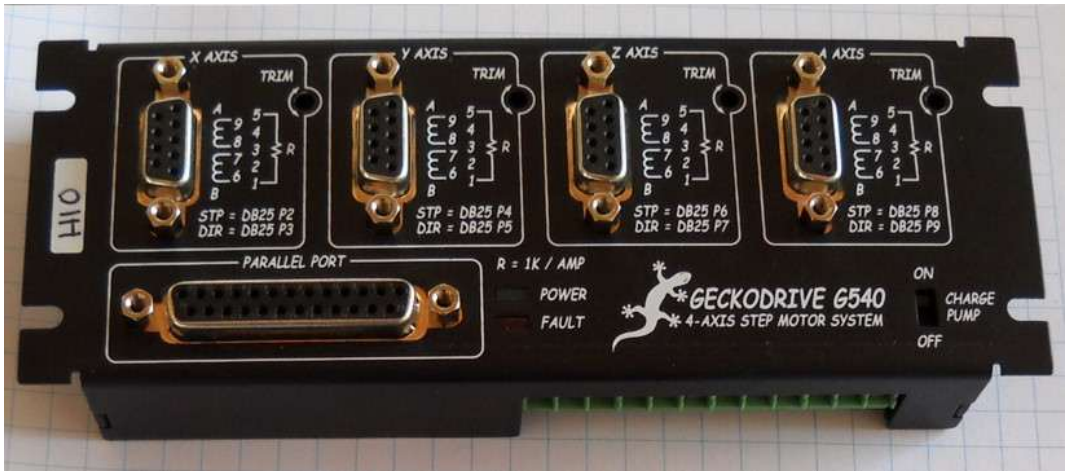

Figure 44 - Geckodrive G540 controller

In order to send this information to the actuators, a motor controller is required that converts inputs in the form of speed and direction commands into current bursts to the phase windings. For the development of the SWIFTER actuation system, a Geckodrive G540 four-channel 10-microstepping controller (Figure 44) operating on 24V DC power was used. The direction input on each of the motor controller channels simply required a high or low voltage signal from one of the DAQ board digital outputs. The speed and distance input, however required a pulse train to be transmitted from a digital output. Each pulse needed to be four microseconds wide, with the speed of the motor determined by the duty cycle of the pulse train, and the distance to move determined by the number of pulses.

This was implemented in Labview by building a Virtual Instrument (VI) with inputs for speed in μm/s, direction, and distance in μm. The direction input sent a single digital 1D sample to the port or ports assigned to the direction input of the one or more actuators to be moved. This changed the state of the port to low or high, and maintained that state until an overriding signal was sent. The speed input was divided by the travel per microstep of 0.635μm, to give the pulse frequency, and multiplied by the pulse width to give the duty cycle. These parameters were then used to generate a pulse train with a base state of low, as required by the motor controller. The distance input was also divided by the travel per microstep, giving the number of pulses required to travel that distance. The now finite pulse train was then sent to the digital ports assigned to the speed input of the actuators to be moved.

Displacement Sensors

The displacement sensor feedback potentiometers are supplied with +/-5V DC power, and wired as variable resistors, with maximum resistance at zero extension, and minimum resistance at maximum extension. This gives a 10V span across the 38.1mm range of motion of the cable, and 260μV/μm. However, due to variations in the power supply, even with voltage smoothing, accuracy can only be guaranteed to fall within ~+/-10μm, however, this is more than sufficient for the purposes of the leading edge actuation. The connections of the potentiometers were wired as differential inputs to the analog input ports of the DAQ board. A Labview VI was then used to record their values. The input from all three potentiometers were collated in a two dimensional array, and then each input averaged over 100 samples to give a mean voltage value.

Electromagnet

The electromagnet operates on 24V DC power, so to control it with the 5V output of the DAQ board, a MOSFET relay board was added. When the DAQ port assigned to the electromagnet was set high, the relay closed and allowed the 24V DC feed to power the electromagnet. When the port was set to low, the relay opened, cutting power to the electromagnet. This was controlled by a Labview VI similar to that of the direction part of the linear actuator VI.

Displacement Sensor Calibration

The displacement sensors each came with a six point calibration from the factory. However, given the small nature of the displacements being measured, it was felt that an independent calibration should be developed. In addition, with two sensors mounted in the step direction, and one in the gap direction, angular corrections would have to be made as the leading edge actuates from position to position. A VI was developed in Labview that would iterate the leading edge through a series of step and gap excrescence positions from zero to the extremes of the range in all directions. First, the leading edge would move from zero gap and step out to 10mm in five steps, momentarily pausing at each one to record the displacement sensor readings. Then, the leading edge would move to a 10mm step in the non-test surface direction, retract the gap to zero, and repeat the move pattern out to the 10mm gap. Then, it would move a 1mm step in the test surface direction, and repeat the pattern. This would continue until it completed the pattern at a 10mm step in the test surface direction. The data was stored in three two-dimensional arrays, which were then imported to MATLAB. The surface fitting tool *sftool* was then used to fit a polynomial curve to the surfaces.

Initial tests with the test rig (to be discussed later in this chapter) showed that the sensors were relatively linear, with only minor curvature resulting from the angular variation with position change. It is planned that a finer initial calibration be carried out when the model is ready to begin testing, and then, for the initial testing phase, a coarse

calibration check be carried out each day until it is verified that day to day variations such as temperature and humidity have no major effect on the calibration.

Actuation Sequences

To this point, the leading edge actuation has only been discussed at the lowest level of code, at which the actuation subVI is given inputs of distance, speed and direction to pass to the motor controller. In order to actuate the leading edge, however, the motors will have to operate as part of a sequence involving the displacement sensors and the electromagnet. There are three different actuation sequences available to the user during operation of the system: Step sequence, Zero sequence, and Gap sequence.

The Step sequence allows the leading edge to be positioned at a desired step excrescence, and zero gap. It consists of three phases. The first creates a leading edge gap of 5mm to allow clearance. The second phase moves the leading edge to the desired step excrescence. The third phase then retracts the gap created in the first phase to seal the leading edge to the body of the model. The Zero sequence is identical to the Step sequence, other than that the second phase is fixed to move the step excrescence to zero, positioning the leading edge in the completely closed configuration. The Gap sequence is designed to create pure gaps, with no step component. It first checks to see whether the step excrescence is at zero. If not, it calls the Zero sequence. Then, it moves the leading edge to the desired gap position. Each of these sequences uses a combination of

step and gap movements. They do this by calling Gap and Step Calculator subVIs. These Calculators take inputs of desired step or gap excrescences, and handle all the operations required to begin, create, and complete that motion.

The first phase of the Gap Calculator takes the input of the desired gap position, and checks whether it is within the safe range of motion in the gap direction. If it exceeds this range, the desired gap is modified to the maximum extended position allowed in the range, provisionally set at 20mm. If the desired gap position is fully retracted, or zero, the desired gap is modified to negative 500µm. With the PTFE gasket in place, this allows the gasket to be compressed to the maximum extent possible, limited by the power of the actuators. It also automatically corrects any minor misalignment of the leading edge between the two gap actuators, as if one reaches the limit before the other, it will simply stall in a safe manner, and the other will catch up. Even though the desired gap is modified to a negative value, the position is still recorded as zero, as the leading edge does not actually retract past this point. Finally in the first phase, the difference between the final desired gap position and the current gap position is calculated, and separated into absolute distance and direction parts.

In the second phase, the electromagnet control subVI is called, and the electromagnet switched off. There is a fixed timeout in this phase, to allow the magnetic field to dissipate before actuation, and avoid the motors stalling. The third phase then calls the actuation subVIs for both gap actuators, feeds in the distance and direction parameters, leaving the speed set at the default setting of 1000µm/s. Once this is complete, the fourth phase begins, which is the reverse of the second phase, activating

the electromagnet. The fifth and final phase of the Gap Calculator checks the previously recorded position of the leading edge in the gap direction against the values from the gap displacement sensor. First, it takes the recorded current gap and step positions and plugs their values +/-10μm into the displacement sensor calibration equations calculated previously. This gives a pair of outputs in volts. The current gap displacement sensor reading is then called. If it falls between these two values, the leading edge is correctly positioned. If it falls outside this value, the leading edge recorded gap position has come out of synchronization with the displacement sensor, and a Gap Sync Error is displayed to the user. If this is a result of a stall, or missed steps, it can be corrected by rezeroing the gap. Otherwise, a recalibration may be necessary.

The Step Calculator operates in a very similar manner to the Gap Calculator. The first phase limits the input desired position to within a safe positive and negative range of 10mm. As there are no hardware safeties such as the electromagnet in the step direction, phases two and four are eliminated. The third and final phase of the Step Calculator checks the recorded position of the leading edge in the step direction against readings from the two step displacement sensors. Both sensors are checked individually against their calibration equations as mentioned earlier. If both sensors are found to be outside calibration, it is likely that the leading edge has come out of synchronization with the displacement sensors, and a Step Sync Error is displayed to the user. If only one of the sensors is outside calibration, it is more likely that one of the actuators has stalled for some reason, possibly as a result of friction, or a component catching internally. This will display a Step Alignment Error to the user. As the step direction does not have a

simple method for validating its position during operation, as with the gap direction, any error displayed would be best dealt with by manual verification, either in the tunnel, or in the hangar after landing, if this occurs during flight testing.

Indicators and Global Variables

The Labview Global Variable feature was used to store any data that needed to be accessed by multiple VIs not in direct communication, such as the current step and gap position information. It was also used to control indicators visible to the user during operation. These indicators include the step and gap alignment and sync errors, which were set to flash a red light four times and then remain lit to attract the attention of the user. The actuation and electromagnet subVIs also communicated their active or inactive state by way of a solid green indicator light. The current step and gap positions are reported to the user by way of a visual representation of the leading edge with sliding indicators along the sides, and a numeric display of the current step and gap in microns.

User Interface

The proposed front panel of the SWIFTER control VI (Figure 45) is the highest level of the Labview VI hierarchy in the control system, and the only screen with which the user would interface. It has a compact design, in order to share screen space with the preexisting flight interface. The actuation controls comprise three primary sections: Operation, Setup, and Diagnostics and Information. To prevent accidental operation of Setup controls during test operations, or of the Operation controls when adjusting the model, the Activate Operation and Activate Setup Controls radio buttons are linked in such a manner that when one is activated, the other is deactivated. This deactivation closes all ongoing operations, and completely locks out the controls in that section. In addition, if any alignment or synchronization errors occur during test operations, the Operation section is also deactivated to prevent further aggravation of the problem, and to give the user time to assess the situation. As is standard practice with Labview, the STOP button also deactivates all sections and resets input conditions before closing the VI.

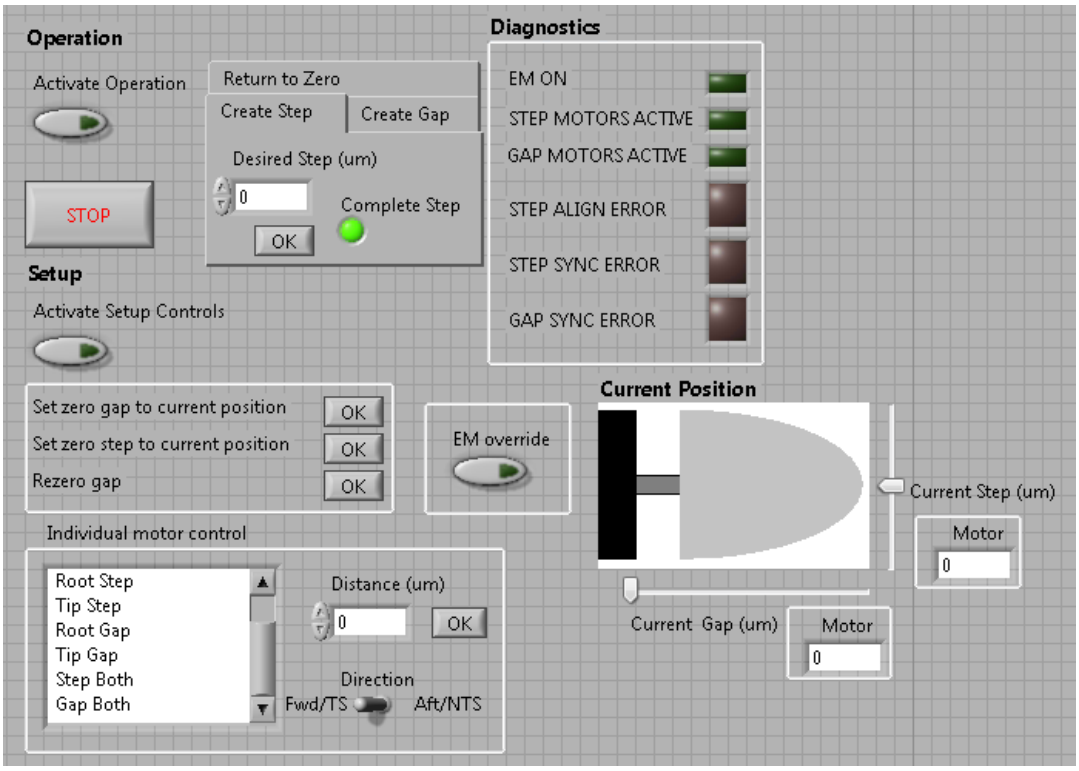

Figure 45 - SWIFTER UI - Actuation

The Operation section is the interface by which the user controls the actuation of the leading edge during test operations, and directly controls the Step, Gap and Zero Sequence subVIs. It consists of a three-part Tab control, which allows only one of the operation tabs – Create Step, Create Gap, and Return to Zero - to be viewed at a time. Both the Create Step and Create Gap tabs have numeric inputs for the desired position in microns, and a radio button to confirm the start of the operation. The Return to Zero tab does not have a numeric input, as its target position is fixed. Once the operation is complete, a green light on the panel flashes four times to notify the user.

The Setup section is designed for use outside of test conditions, for operations such as when the leading edge is being realigned, or the step excrescence zero position is being set. It has three primary functional areas. The first is the electromagnet override. As the actuators are able to be controlled individually in Setup, unlike in the Operation section, the lower-level actuation subVIs are being used. As a result, the automatic powering on and off of the electromagnet is unavailable. Therefore, deactivating the electromagnet is necessary for all Setup operations. The second is the individual actuator control panel. This subsection allows the user to move each of the four actuators individually or in gap or step pairs to achieve perfect alignment of the leading edge with the body of the model before commencing operations. It has a Listbox selector by which the desired actuator or pair of actuators for motion can be selected, a numeric input for distance to be moved in microns – unlike the operation input, in which the final desired position is entered, a direction switch, and a radio button to confirm the start of the motion. The third and final section is the position updater. Once the leading edge is set to a zero step and zero gap - or relative zero gap when using gap inserts - configuration by the user, the current step position and current gap position variables used by the operational Step and Gap Sequence subVIs can be updated to zero at this reference condition.

The Diagnostics and Information section consists of the indicator panel by which the user is informed of actuator and electromagnet power state, as well as any alignment of synchronization errors, and the Current Position graphic, showing the current leading

edge excrescence configuration by way of sliding indicators and numeric readouts in microns.

Actuation System Test Rig

As the SWIFTER model was still in production during the development of the actuation control system, an alternative system had to be developed to test the proposed Labview code and interface hardware. This test rig (Figure 46) would be required to test the linear actuators and the displacement sensors. It was not seen as necessary to test the electromagnet, as its control was elementary. In order to best replicate the application, it was decided to use two actuators mounted at right angles, with the second actuator mounted on a traversing platform driven by the first actuator. This was achieved by way of a Dry-Lin TW-01-15 linear rail guide available from the FRL surplus.

For these initial tests, only one Unimeasure ZX-PA displacement sensor was acquired. This was used to measure the displacement of the shaft of the second actuator relative to the test rig baseplate. To measure the displacement of the first actuator shaft and the traversing platform, an Omega LP-803 solid shaft linear potentiometer displacement sensor was used. As the connection point on the traversing platform did not move transverse to the shaft of this sensor, the lack of two-dimensional freedom available with the Unimeasure sensor was not an issue.

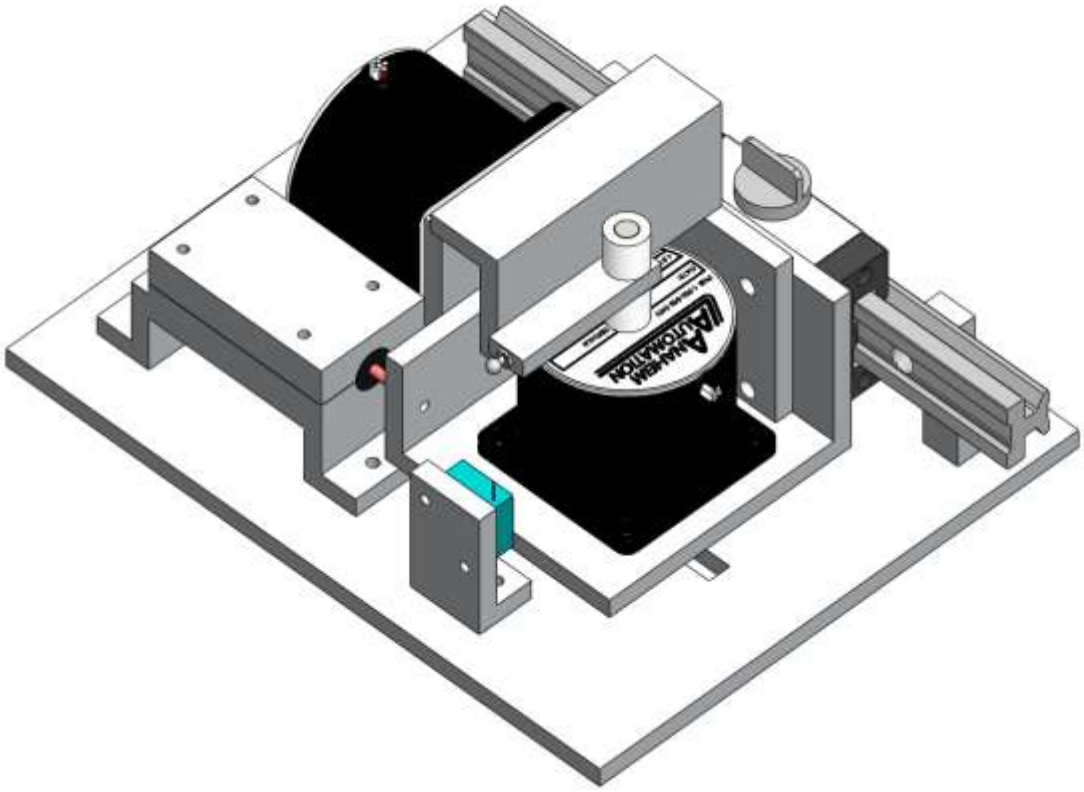

Figure 46 - Actuation system test rig

As the shaft of the second actuator was not fixed rotationally, it could have spun freely when active, instead of giving pure axial motion. To solve this problem, a rectangular arm was bolted to it. This arm sat against a vertical plate bolted to the traversing platform, and prevented rotation of the shaft. It had the secondary function of providing a connection point for the end of the displacement sensor cable. The test rig structure was manufactured in the Low Speed Wind Tunnel (LSWT) machine shop from 6061-T6 aluminum.

CHAPTER V

HEATING SYSTEM

Test Surface Heating

As mentioned in Chapter II, during flight testing, the Reynolds number range of interest means that not all flights will involve a dive in the data acquisition phase. This has the advantage of extending both the duration of the test flights, and the range of operational conditions in which they can take place. The disadvantage of this, however, is that the atmospheric thermal gradient can no longer be used to heat the model and create a visible transition front on the IR image. Similarly, when testing in the wind tunnel, no thermal gradient is available.

To solve this problem, it was decided to actively heat the test surface of the model. Heating the test surface to a uniform temperature prior to the test operation, and then switching off the heater and allowing the airflow to cool the test surface would, in effect, be the opposite of the current method in use in flight. Instead of having a uniformly cold-soaked model heating at different rates dependent on the laminar or turbulent flow condition, there would be a uniformly-heated test surface being cooled, with the only practical difference being the inversion of the colors on the IR image.

The four primary design considerations when deciding how to control the temperature of the test surface of the model were that the system must be internal, so as not to effect the flow over the test surface, that it must be unaffected by the elements, that it must be light enough to use in flight, and that it must be power-efficient enough to operate on the available power from the aircraft. Several methods of controlling the surface temperature of the model were considered, including water cooling, as had previously been used on models in the KSWT. However, this option was ruled out due to weight limitations in flight, in addition to the complexities of running a water system in the vicinity of the electrical leading edge control hardware. It was decided to heat the test surface of the model by way of electrical resistance heater elements. These would be applied to the inside face of the test surface, and power applied until the outer surface had reached the desired uniform temperature.

To estimate the power requirements of the resistance heaters, a high-end thermal delta of 10^{o}C, and a warm-up time of 180 seconds were chosen. The formula for warm-up power is given by

$$P(watts) = \frac{mC_p(T_f - T_i)}{t}$$

where m = mass of the test surface (g)

C_p = Specific heat of aluminium (J/g/^oC)

T_f = Final temperature (^oC)

T_i = Initial temperature (^oC)

t = Warm-up time (seconds)

Allowing for 20% losses through various mechanisms gives an estimate of 800W required, which is within the capabilities of the aircraft power supply. As noted above, this is a high-end estimate, as the required thermal delta will likely be lower, on the order of 2-5^oC.

When the initial studies were carried out, the test surface had a uniform thickness, which greatly simplified the heating system. However, after the leading edge displacement studies were completed, the forward region of the test surface was thickened. This created four distinct surfaces with different thicknesses to the exterior of the test surface to be heated. In addition to this, the test surface had several pylons and hardware mounting points that would be unable to be heated directly (Figure 47). However, these are isolated, and heat will spread into them from the surrounding areas, reducing the size of the unheated spots on the test surface. IR images from previous testing with the SWIFT model also show that features such as ribs do not have a large impact on overall image quality. In order to ensure uniformity across the entire test surface despite the areas of different thickness, the areas will have to be separately

controlled and set to the target temperature. As the areas are also of varying sizes, the rate at which they heat will have to be adjusted to ensure that a uniform temperature is achieved across all areas at roughly the same time.

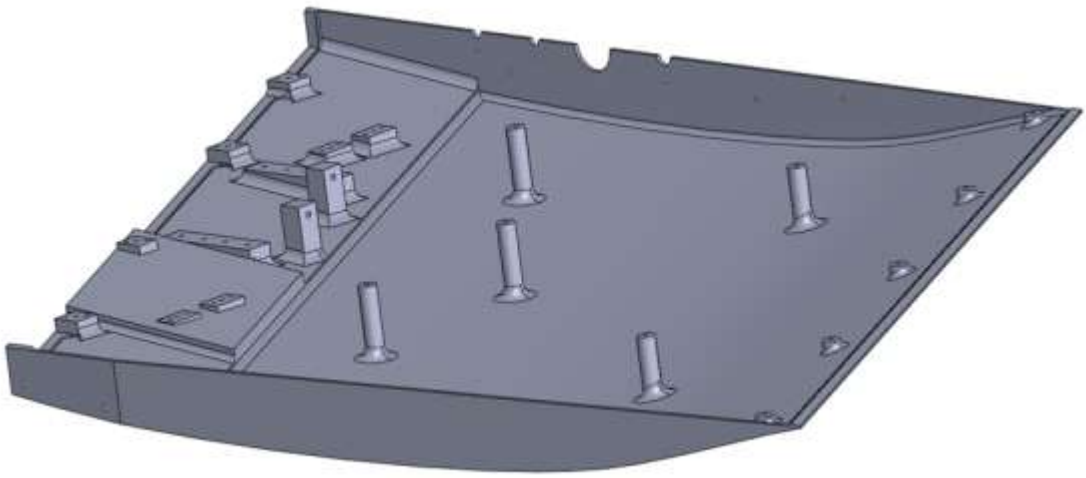

Figure 47 - SWIFTER test surface interior

Feedback and Control

The temperature of the heated areas will be measured with three-wire Resistance Temperature Detectors (RTDs), which have a linear relationship between temperature and resistance. These sensors will be mounted on the inside face of the test surface with the heating elements. The three-wire configuration minimizes the effects of the lead wire resistance on the reading. RTDs have an advantage over thermocouples in that they do not require special wiring from the sensor to the control unit, which is useful when mounted on the O-2A, as the standard connectors can be used. They are also more stable and accurate, in general, than surface-mounted thermocouples, which can drift over time. One disadvantage of this configuration is that the temperature on the exterior of the test surface is not directly being measured. If this is found to be required during testing, a possible solution is to use non-contact IR thermocouples. These single-pixel sensors can be mounted remotely, e.g. in the window of the O-2A cabin, and directed at the centre of each of the heated areas to provide a definitive measurement of the test surface temperatures.

To control the heating of the test surface, a Watlow EZ-Zone digital controller system will be used. This system consists of three modules – an RMC control module, an RME expansion module, and an EZ-RUI user interface module. The modules operate on 24V DC power, and draw 7W each. The RMC control module has four bays (Figure 48), each of which contains an input connector to which the RTD can be wired. The

RME expansion module has four bays, of which two contain a dual 10A Solid State Relay (SSR) output for four outputs in total, and two are left empty. 110V AC supply power is connected to these relays, and then out to the terminals of the heating elements. The 10A limit is more than sufficient to provide the power required to heat the elements, and the output power can be scaled to suit the application. A Quencharc capacitor connected across the elements protects the circuitry from the counter electromagnetic force when the elements are depowered. The EZ-RUI interface (Figure 49) will not be used as the primary programming interface in this application, but will serve as a display of current element temperatures or setpoints, and any errors that may occur.

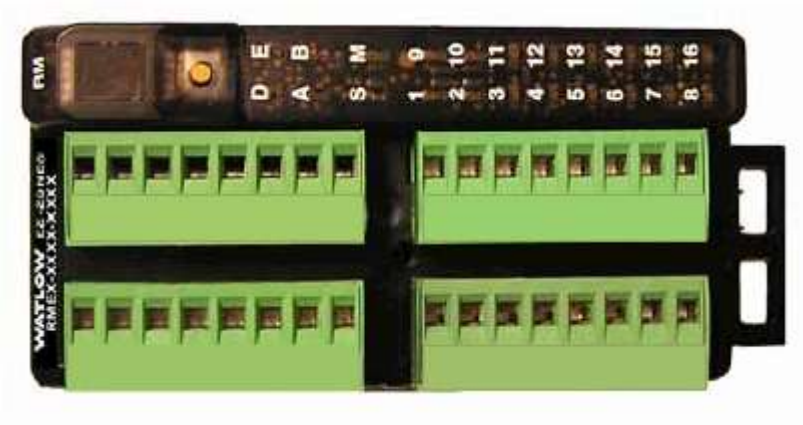

Figure 48 - Layout of RMC and RME interfaces

Figure 49 - EZ-RUI interface

The controller system interfaces with the laptop through a USB to RS-485 serial port adapter. Watlow provides its own EZ-Zone Configurator software to allow the controllers to be easily programmed, and this interface is useful for initial setup and calibration of a full set of variables. However, for operation during tests, it is preferable to integrate the control of the heating system into the Labview user interface. To do this, Watlow provided an example Labview VI for writing to and reading from the controllers. Although the example VI itself was not well suited to the application, it contained subVIs to control communication over the RS-485 serial connection, which could be integrated into the SWIFTER control VI.

These subVIs allowed the communications port to be opened, written to, read from, and closed. The Open and Close subVIs required only an input of which communications port to operate. The Read and Write subVIs took inputs of zone, parameter, and instance, and for Write, value. Zone determined which controller module would be targeted. Parameter specified which parameter was to be selected, and instance

specified which individual input or output was to be read or written. A complete list of control parameters is available in the RMC and RME user manuals. For the proposed Labview code, only the parameters expected to need to be controlled during test operations were made available. These were setting and checking the target temperature, changing the control loop state on and off, and monitoring the heater power level.

To avoid the user having to remember a list of numeric parameters and associated input values, parameter control was integrated into the user interface using a Listbox selector for the parameters, a numeric input for the target temperature, a selector switch for control loop activation, and an array of numeric readouts to display the current values of the selected parameter. It is planned to add a realtime updating graphic display of the current and target temperatures for each heated area, both to allow verification that the target temperature has been reached and maintained, and to allow the user to monitor how the controller is achieving this temperature, and whether the rate or damping need to be adjusted. To set up and calibrate the heating system, however, would require more parameters to be controlled than just those added to the Labview VI. These include calibrating the Proportional Integral Derivative (PID) control variables to determine how the heating elements approach and maintain their target temperature, setting the upper and lower power limits on each element to ensure that the surface reaches a uniform temperature at an even rate, setting the sensor input type and units, and setting any offsets that are found to be required. All of these tasks, as mentioned above, are more easily accomplished using the Watlow EZ-Zone Configurator software.

CHAPTER VI

WALL LINER DESIGN

Function and Theory

When a model is installed in a standard rectangular wind tunnel, the flow past it is quite different from the flow that it would experience in a free flight condition. This is due to the finite cross section of the test section, whose walls exert an influence on the flow near them, and change the pressure distribution across the surfaces of the model. In a wind tunnel such as the KSWT, with a cross section area of 1.4m x 1.4m (4.5ft x 4.5ft), an airfoil section model such as SWIFTER, with a relatively large 1.37m (54 inch) chord, will experience significant pressure distribution effects, which produce a highly three-dimensional pressure pattern. Additionally, three-dimensional boundary layer instabilities can be introduced, with effects on transition pattern. Other effects include turbulent wedges propagating from the junction between the leading edge and the upper and lower walls. These wedges grow inwards at a 12^{o} angle, reducing the area on the test surface of the model where representative data may be obtained.

To counter these effects, and obtain a spanwise uniform flowfield across the model, wall liners can be installed in the test section, at each end of the model, that follow the curved streamlines of the flow around an infinite-span version of the airfoil in a free flight condition. For this proposed wall liner design for SWIFTER in the KSWT, the side walls will remain flat, and not bulge to follow the contours of the flow over the surfaces, as this makes taking observations and measurements of the conditions difficult. Dagenhart & Saric (1999), show that the influence of the sidewalls on the pressure distribution over the model surfaces is not negligible, but that the pressure distributions remain qualitatively the same when the wall interference is included in the design of the wall liners.

Streamlines to Solids

To create a zero-lift condition, it was decided to set the angle of attack of the model in the tunnel at negative 2^o. Streamlines at 30^o angle of incidence to the infinite airfoil model replicated the sweep of the model. Using ANSYS ICEM to create a grid, and then ANSYS Fluent to model the flow, Matthew Tufts generated a set of streamlines distributed from both surfaces of the model to the tunnel side walls, and extending far upstream and downstream of the model. To import these streamlines to Solidworks, they were converted to a comma-delimited .sldcrv format. As Solidworks could not handle the large number of points in the streamline files, the point density of the streamlines

was reduced from ~160,000 per streamline to ~1,000 by filtering the data to a 5mm spacing tolerance. This still provided enough resolution for smooth curves, and was on the same order as the number of points used when designing the wall liners for use with the ASU (67)-0315 model.

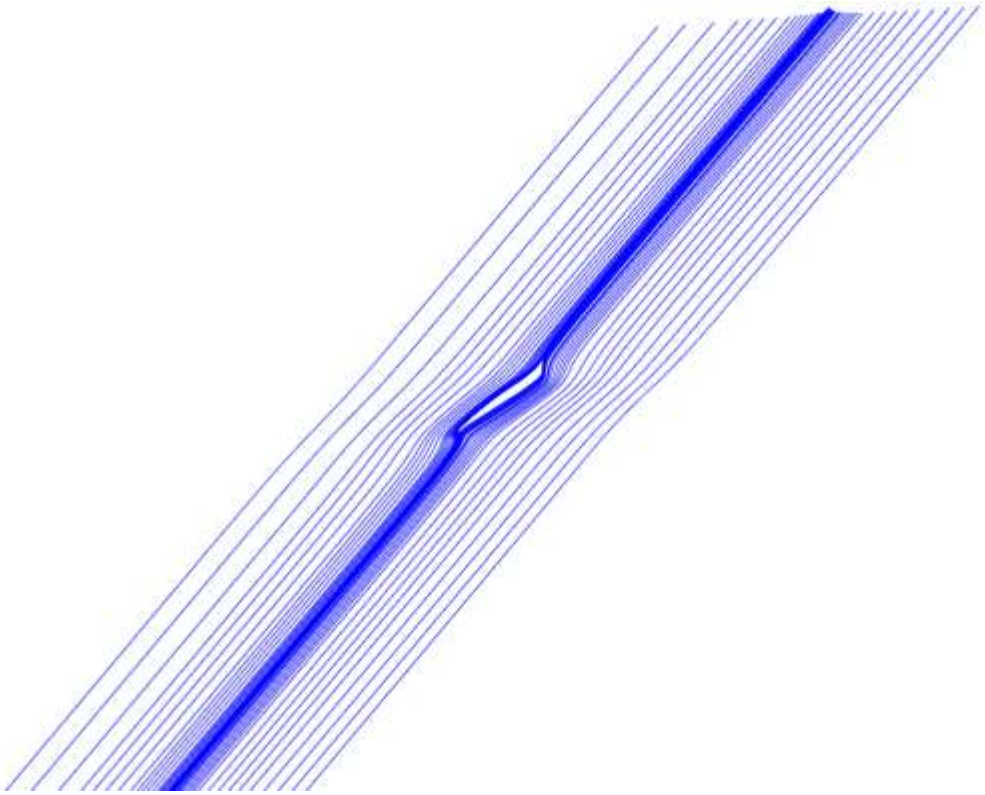

Figure 50 - Streamlines around infinite SWIFTER airfoil (Flow from bottom left)

After importing the set of streamlines, seen in Figure 50, the next step was to create a smooth surface. This was accomplished using the Surface Loft tool, which calculates a smooth surface curve to link a series of line curves. The surfaces were created in two halves – the test surface and non-test surface. Some streamlines in the region of highest curvature near the model were omitted in order that the surfaces could be solved. Comparison of the finished surface with these curves showed no deviation of note from their path. As the curves were imported at a 30^{o} angle of incidence, a new reference plane was established parallel to the plane of the flow to which the wall liners would be made orthogonal. At this point, the design was split into upper and lower wall liner files. The surface used by both would be identical, but for the upper wall liner, the lower face of the streamsurface would face out, and the upper face for the lower wall liner. The procedure, listed below for creating the solid wall liners, is otherwise identical.

To create a solid part for the wall liner, first the innermost curves of the streamsurfaces were extruded downwards at 30^{o} along the axis of the model. A perimeter box, with the dimensions of the test section was then added, and the streamsurfaces trimmed to this. The perimeter box was then trimmed to intersect the extruded inner curves of the test side. The only remaining open face of the box was then closed using the Plane Surface tool, and then a solid part created using the Knit Surface tool. The procedure was then repeated to create the non-test side solid part.

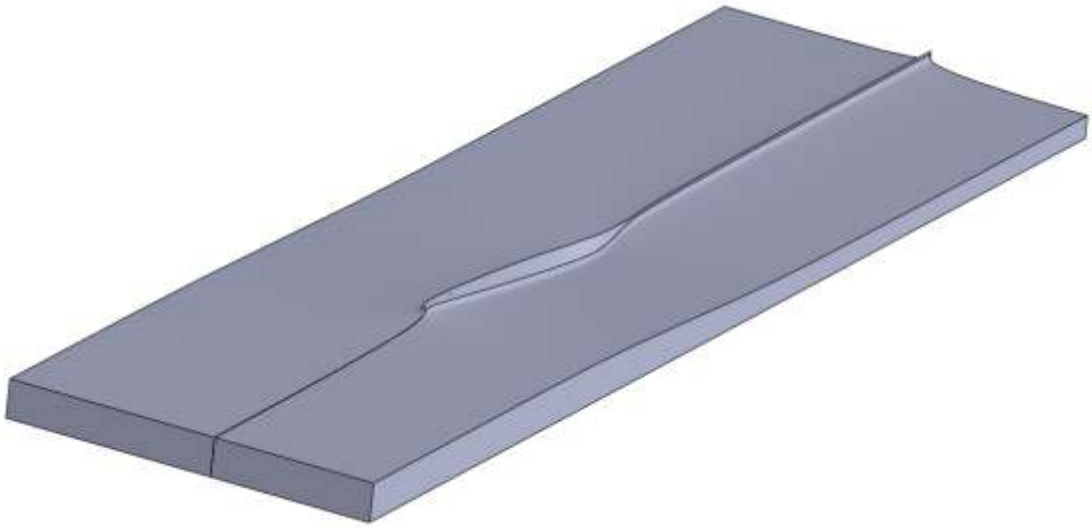

Figure 51 - Lower wall liner solid parts

The thickness of the wall liners was determined by the contraction cone fairing upstream of the test section, previously installed for use with the ASU (67)-0315 model and wall liners. In order to have a smooth flow over the interface, the wall liners would have to match the distance from the upper and lower walls of the tunnel to the fairings. The construction of new contraction cone fairings was considered, but as successful operation of the tunnel, with no choking effects encountered, was well documented in previous tests with that contraction ratio, it was decided to keep it the same. This had the additional advantage of simplifying procedures when switching between testing with SWIFTER and ASU (67)-0315, as fairings would not need to be changed out. As the ASU (67)-0315 had a 15cm wider span than SWIFTER, matching the liner thickness to

the existing contraction cone fairing meant that the wall liners would sit too low to the floor and ceiling of the test section to properly cover the root and tip of the model along the full chord. To solve this issue, an airfoil spacer, shaped to the OML of SWIFTER was designed to fit to the root end of the model and bridge the gap (Figure 52). The gap at the ceiling of the test section was small enough not to require a spacer, as taping the model and liner interface would cover the slight gap at the trailing edge of the model without difficulty.

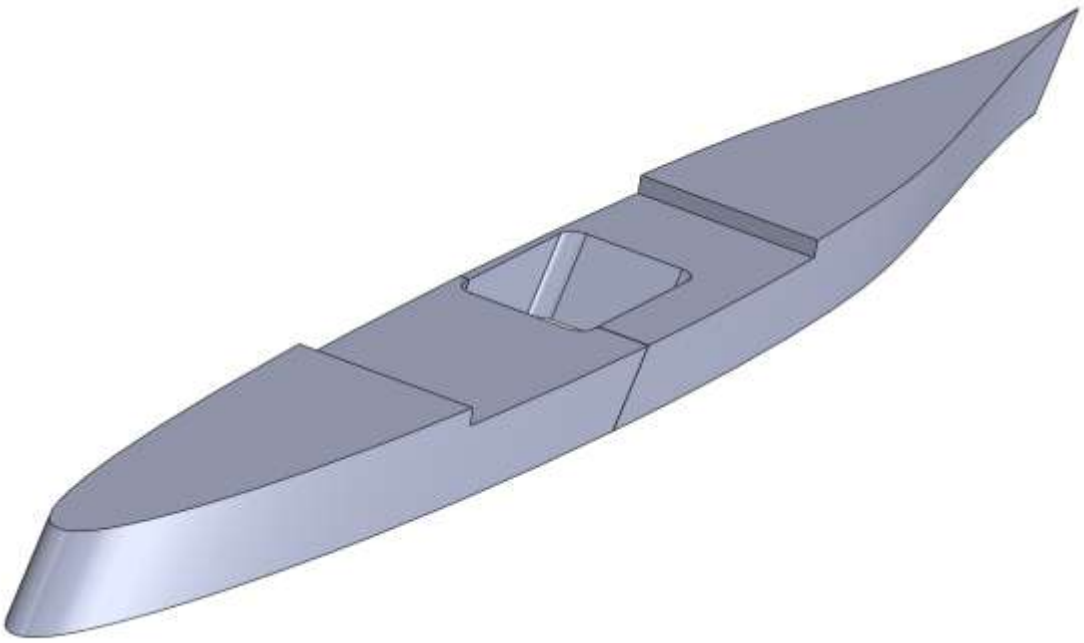

Figure 52 - Airfoil spacer

Unlike with previous models, the nature of SWIFTER required that some modifications be made to the wall liners. At both the root and tip of the model, a section of wall liner was cut back from the leading edge to allow the actuation system to function throughout its range (Figure 53). Taping between the liner and the leading edge would prevent any unwanted sharp steps from being presented to the flow. Two channels were also cut into the test and non-test sides of the upper wall liner, perpendicular to the leading edge interface, to allow gap inserts to be maneuvered into position while the model is installed in the wind tunnel. When not being used for this purpose, the channels will be taped over to prevent any disturbance to the flow.

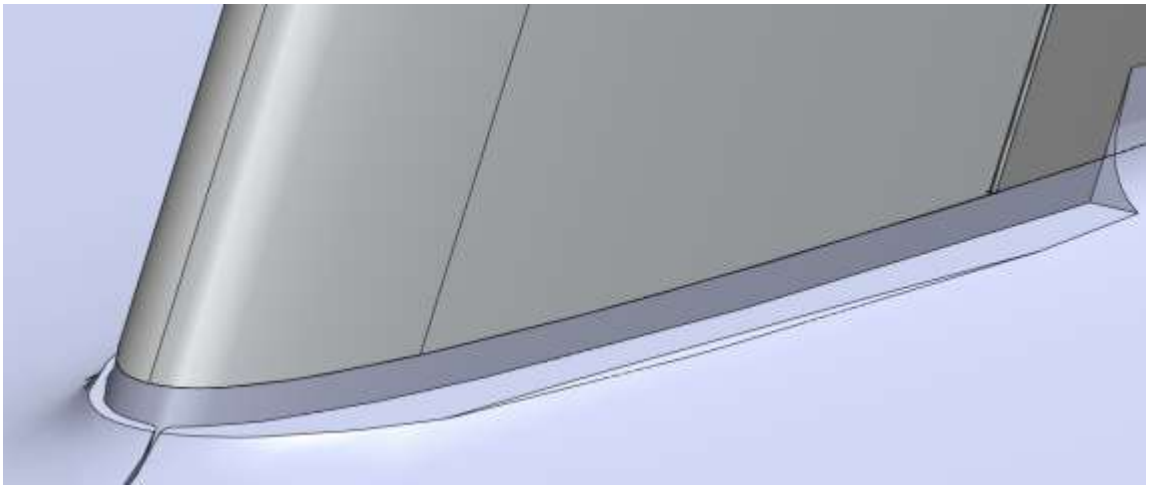

Figure 53 - Wall liner leading edge cutaway

Splitting to Sections

At this point in the design, the wall liners consist of four monolithic blocks – upper and lower, test side and non-test side. In order to construct the wall liners in a practical manner, there are four main restricting factors that need to be considered. First, the liner sections have to be split into quadrants, top and bottom, in order to allow them to be inserted around the model once it is installed in the test section. Secondly, the stock foam material from which the wall liners will be constructed is available in 2.44m x 1.22m (8ft x 4ft) billets, which are not long enough to completely construct a full-length quadrant. Thirdly, the limitations of the foam cutting machine, which can only cut material up to 7.5cm (three inches) thick. Finally, the strength of the foam itself - the material can only be cut so thin before it becomes at risk of failing under its own weight before all the pieces can be assembled.

The procedure developed to satisfy these restrictions was to take each quadrant section individually, and, starting at the outer flat face and moving inwards towards the profiled surface, divide the quadrant into a series of layers. The first layer piece would be made as thick as practical to minimize the number of foam sheets required, and yet not leave the remaining section be so thin in some pieces that it would risk failure. The remaining section would then be inspected to determine what thickness slices could then be taken to divide it into pieces that would both fit into a standard thickness foam sheet,

and again be thick enough in all areas not to fail. Each quadrant had to be inspected individually, due to the varying contours across the surfaces of the wall liners.

The lower wall liner, due to the shape of the streamlines aft of the model, had a thin ridged section from the trailing edge of the model to the aft end of the test section. Again, due to the thin nature of this ridge, material strength had to be considered. The ridge was very tall relative to its width, meaning that there would not be enough thickness within the three inch maximum to provide a rigid base section along the full length of the quadrant. It was therefore decided to split the uppermost layer into a series of short pieces, no more than 0.6m in length. Additionally, one piece had to be split into two laterally due to a narrow section in the center of the non-test side quadrant.

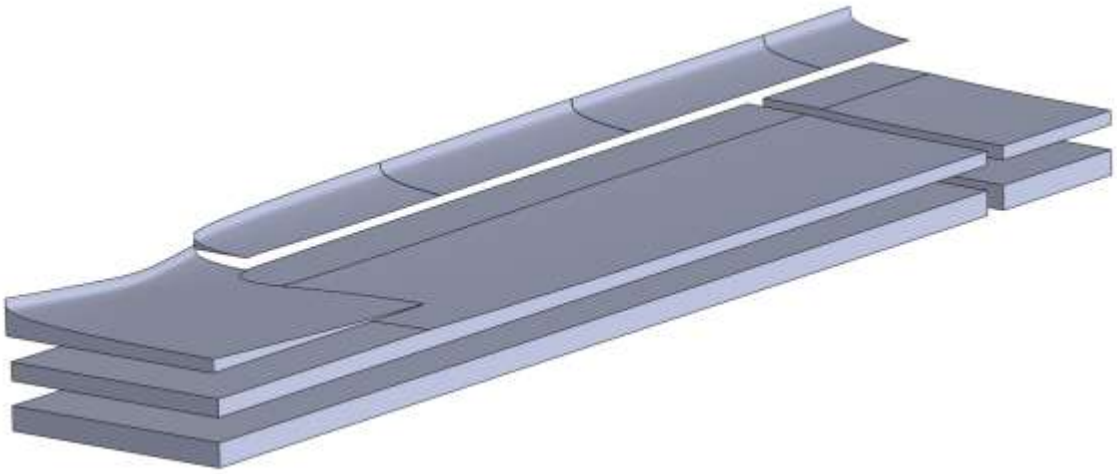

Figure 54 - Exploded view of the lower wall liner, downstream test surface quadrant

Due to the 30^{o} sweep of the model, the quadrants forward of the model in the upper wall liner, and the quadrants aft of the model in the lower wall liner exceeded the maximum 2.44m length available in the stock foam billets, and were required to be split into two sections through all the layers longitudinally to compensate. The airfoil spacer was divided into four pieces – upstream and downstream, test and non-test side, which would each be permanently attached in position to their respective quadrants of the lower wall liner to simplify assembly. A complete list of wall liner pieces, dimensions, and related information is included in Appendix A.

A system of nomenclature was created to keep track of the large number of final pieces. For the first part of the name, the piece would be labeled **Upper** or **Lower**, for upper or lower wall liner. Next, it would be labeled **TS** or **NTS** for test or non-test surface. Then would come **A** or **B,** for upstream or downstream. The layers, referenced from the outermost, would be numbered **1**, **2**, **3** etc. If the layer was sectioned along its length, the pieces would be labeled **a**, **b**, **c** etc., referenced from the upstream edge of the part. Finally, if the section was split laterally, the parts would be identified by **in** or **out**, relative to the model. For example, the upper surface, non-test side, upstream, layer 2, upstream piece, and the lower surface, non-test side, downstream, layer 3, second most upstream, model side piece would be respectively denoted as **Upper NTS A 2a** and **Lower NTS B 3b in**.

Assembly and Finishing

When all the wall liner pieces have been manufactured, the following procedure is proposed for their assembly and finishing. To start, the pieces will be dry-assembled in the test section around the model. Any minor dimensional irregularities and fit issues can be dealt with at this point. Once all the pieces have achieved a satisfactory fit, each quadrant will be permanently assembled using a heavy duty construction adhesive. Next, all surfaces of the quadrants will be coated with an epoxy-microsphere blend, creating an impermeable and easily sanded surface to provide a good substrate for fibreglassing. Two layers of fiberglass cloth will then be applied, first a 10oz/sq yd plain weave, and then a 3oz/sq yd satin weave for an improved surface finish. This will provide a hard outer layer to protect the wall liners from damage during use or storage, and allow tunnel operators to put their weight on them when working on the model. Finally, the wall liners will be finished with a coat of flat black paint.

CHAPTER VII

PRELIMINARY TESTING

In order to gain some experience of step excrescence testing before the SWIFTER model was completed, and to develop some initial avenues of investigation for the actual experimental testing stage, it was decided to use the ASU (67)-0315 model in the KSWT to investigate step effects. Steps would be created by applying material to the test surface of the model to create a uniform forward or aft facing step configuration. The ASU (67)-0315 model (Figure 55) is a 45^{o} swept wing model with a chord of 1.83m (72 inches), and a pressure minimum at 71% chord. The leading edge to 10% chord is constructed of solid aluminum, and the main body has a fiberglass skin to reduce weight. The model has a 0.76m (30 inch) interchangeable aluminum leading edge section centered at mid-span, which extends back to 20% chord. For this experiment, a solid leading edge section would be used.

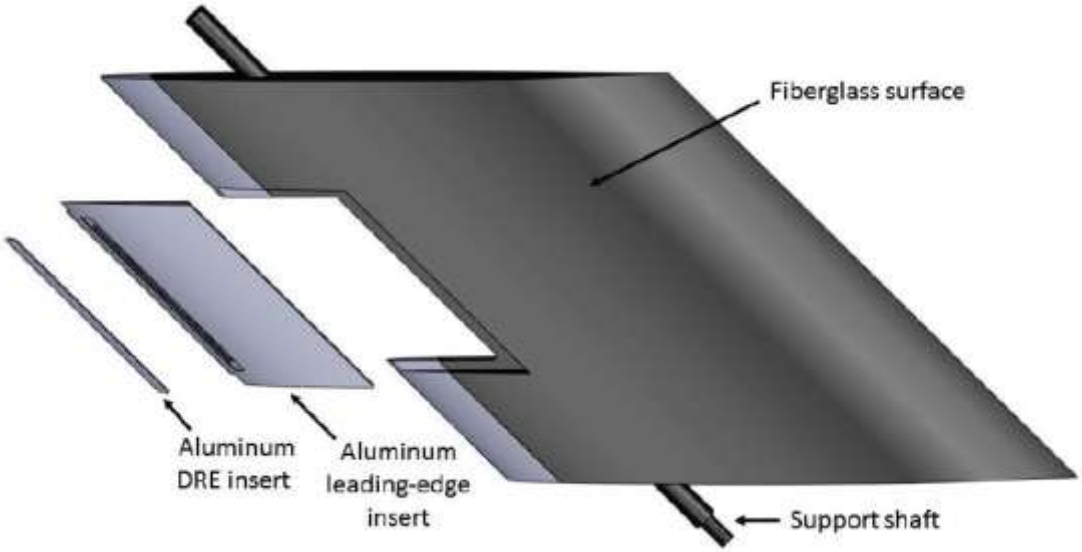

Figure 55 - ASU (67)-0315

Material and Preparation

To create the uniform step excrescence on the model test surface, several materials were considered. A hard rapid-prototyped polymer sheet formed to the surface contour of the model was investigated, however as the facilities at Texas A&M were unable to produce parts of the size required, this idea was discarded. A conformal appliqué material such as foam or rubber sheeting was then investigated. The advantage of being able to order a large quantity of material on a roll, and create various configurations simply by cutting to size and applying to the model seemed an attractive proposition. Samples of various materials were therefore acquired for initial testing purposes. These

included closed-cell foam and neoprene rubber, with adhesive backing for ease of application.

To ensure that the surface finish of the appliqué material would not itself cause transition on the test surface of the model, the roughness of the materials was investigated using a Mitutoyo SJ-400 Surface Roughness Tester. This unit is a stylus based profilometer and can be calibrated by the user to give sub-0.01μm accurate measurements. Initial surface measurements of the foam and rubber material found them to be well outside acceptable limits for boundary-layer testing, with average RMS measurements of greater than 15μm recorded for both materials. Sanding and polishing the rubber material saw incremental gains. Adding a layer of Kapton film to the surface, however, dramatically reduced the roughness values. The foam material, with a layer of Kapton smoothly applied to the surface gave average RMS values of 3μm, while the rubber material gave average RMS values of 1μm roughness. Therefore, the rubber material, with a layer of Kapton film across the surface was selected.

Application testing was conducted prior to installing the material on the ASU model. It was found that the adhesive on the back of the rubber did not adhere uniformly, and left pockets of air trapped between the adhesive and the sheet. These had to be individually slit open and flattened as the sheet was being applied to the surface. Some minor surface imperfections did remain. However, due to their low amplitude and smooth contours, they were not seen to have a noticeable effect on transition during testing. As the adhesive tended to leave a residue on the surface after removal, it was

decided to apply a layer of Kapton tape to the test surface of the model prior to the application of the rubber sheet to protect the finish.

Experimental Design and Techniques

As the experiment would be conducted in a break between other testing programs on the ASU model, to avoid any risk of scratching the surface, it was decided to work only with a forward-facing step, with its leading edge located at 22% chord, slightly aft of the highly polished region forward of 20% chord, and extending back to aft of 65% chord. The rubber material created a step height *k* of 1.6mm. Transition detection for the experiment would be conducted using naphthalene flow visualization. The technique works on the principle that at or near room temperature, naphthalene sublimes at a rate proportional to the shear stress experienced. As turbulent regions have higher shear stress, the sublimation will happen faster than in laminar regions, and will provide a defined image of the transition front, or any wedges caused by surface imperfections or debris. A coat of naphthalene would be applied immediately before each test run so that the minimum amount of material would sublime prior to the tunnel coming on condition, thus maximizing the contrast visible between the regions. Once the test was completed, the tunnel would stay running until all the naphthalene had sublimed. To apply the naphthalene to the surface of the model, first, the naphthalene crystals were dissolved in acetone until the mixture saturated. The mixture was then sprayed onto the surface of the

appliqué material, moving towards the aft of the model, with the spray pattern moving in the spanwise direction and parallel to the leading edge in order to avoid visual confusion with transition patterns as a result of variations in thickness of the application that may occur as a result of overlapping lines of spraying.

With the 1.6mm *k* excrescence, the KSWT range of operation provided an ideal range of operating speeds to produce Re_k values normal to the leading edge on the same order as the Northrop SETS tests. Data were available from previous tests with the ASU model for chord Reynolds values of $1.6x10^6$, $2.4X10^6$, $2.8X10^6$, and $3.2X10^6$ from which to calculate these. Using the formula:

$$Re_k = \frac{u_k k}{\nu_k}$$

where u_k is the velocity observed at height *k* above the surface in an undisturbed boundary layer, and ν_k is the viscosity at that same location, the Re_k values normal to the leading edge for the chord Reynolds numbers provided were found to range from 647 to 2889. As the values changed in a linear manner, they were then interpolated to provide intermediate values, and extrapolated downwards for lower values (Figure 56). Test runs were conducted at nine different chord Reynolds numbers, listed below in Figure 57 with corresponding values for Re_k and Re_{xk}, the Reynolds number at the chordwise location of the step.

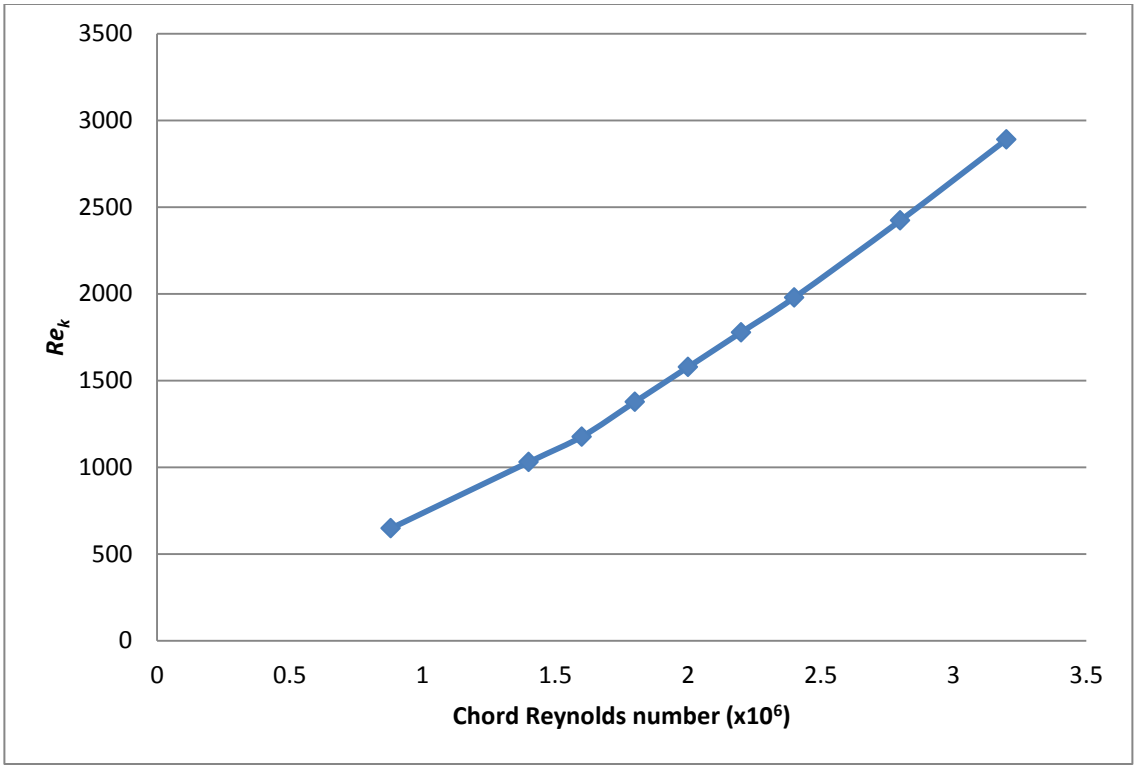

Figure 56 - Re_k v chord Reynolds number

Re_c $(X10^6)$	Re_k	Re_{xk} $(X10^6)$
0.88	647	0.19
1.4	1029	0.31
1.6	1176	0.35
1.8	1376	0.40
2	1577	0.44
2.2	1777	0.48
2.4	1978	0.53
2.8	2422	0.62
3.2	2889	0.70

Figure 57 - Test run Reynolds values

Experimental Results

Due to a combination of heavy naphthalene application and spraying up to the leading edge of the appliqué material, the early test runs provided little useful information. Wedges immediately formed from the leading edge of the material, which were believed to be as a result of naphthalene crystal buildup. To counter this, later runs

only sprayed naphthalene from 30% chord aft, and the leading edge was inspected for any unwanted debris before each run commenced. Despite these efforts to improve the quality of the naphthalene application, a definitive transition front was not identified at any tested chord Reynolds number. As normal transition on the model, without the added appliqué excrescence sheet had been recorded at 55-60% chord at 2.8X10^6 Re_c, it is very unlikely that the front would have moved aft off the sheet.

Figure 58 - Wedge and streak pattern at 2.8X10^6 Re_c

The best images were recorded at $2.8X10^6$ Re_c, and showed multiple distinct wavelength structures repeated across the span of the model (Figure 58). All of the wavelengths were at or less than 12mm, the most unstable wavelength for the ASU model. It is unknown whether these structures result from the existence of the step on the surface of the model, or if they were caused by minor irregularities in the vertical face of the step, which resulted from the cutting of the rubber material or application of the Kapton film, but their existence does serve as a reference for the tests with the SWIFTER model.

Also noted during testing was the fact that the due to the curvature of the surface of the model, the angle of incidence of the flow on the face of the step would not be orthogonal, as with the flat plate tests that had previously been conducted. This would lead to an effectively different step excrescence height. Therefore, the local flow velocity component and the resultant Re_k values of any tests with the SWIFTER model will need to be adjusted for direct comparison with those previous studies.

CHAPTER VIII

CONCLUSIONS AND RECOMMENDATIONS

Leading Edge Actuation Control System

A control system was proposed to control the actuation of the leading edge of the SWIFTER model, and create step and gap excrescences at precise specified locations. A hardware interface, with a National Instruments USB-6341 DAQ board, a voltage smoothing circuit for the displacement sensors, and a Geckodrive G540 motor controller for the linear actuators was assembled. A structured Labview user interface was then created to allow the test operator to control the leading edge from the flight laptop. This consisted of a hierarchical series of Virtual Instruments integrating all the hardware controls required for the test operations and carrying out all calculations and checks required to safely and efficiently move the leading edge as requested. Labview code was also created to develop a calibration set for the displacement sensors which could then act as a reference for day to day calibration variations.

Going forward, the proposed user interface would need to be integrated into the existing flight VI in a manner which allows all pertinent information and controls to be displayed on screen at once. Once the SWIFTER model is fully operational, variables such as timeouts for electromagnet power cycling, number of samples for the

displacement sensors, and safe limits on actuation ranges in the step and gap directions could then be optimized. The calibration of the displacement sensors should be checked daily until it is verified the environmental variables have no major effect on the calibration. A refinement of the linear actuator control VI, taking speed ramping into account, as opposed to the instant speed setting of the current method, could lead to smoother operation and less wear on the hardware components.

Test Surface Heating System

An active heating system for the test surface of the SWIFTER model was developed in order to allow IR thermography data to be acquired both in flight without the creation of a thermal gradient from a dive, and in the wind tunnel. This system involved heating the inner face of the test surface by way of electrical resistance heater elements. Due to the discrete variations in thickness across the inner face of the test surface, the heater elements must be controlled by separate loops for each of the areas to produce a uniform temperature across the external face of the test surface. The temperature of each area of the test surface will be monitored by way of surface-mounted RTDs. The heating of the surface will be controlled by a Watlow EZ-Zone digital controller system, consisting of an RMC control module with inputs for the RTDs, an RME expansion module with four 10A Solid State Relays to control power to the resistive heating elements, and an EZ-RUI user interface module, which can display pertinent information and error messages

to the test operator. The controller system connects to the flight laptop by way of a USB to RS-485 serial port adapter. Proprietary configuration software by Watlow can be used for initial setup purposes, and control can be integrated into the Labview user interface to allow target temperatures and other parameters to be adjusted and heating to be started and stopped during test operations.

Going forward, the proposed heating system user interface can be integrated into the existing flight VI, and refined to allow control of all pertinent parameters to be easily monitored and adjusted by the test operator. The addition of a realtime display of current and target temperatures for each area would be recommended. Once the system is operational, variables such as power applied to each heated area, the rate of heating each area, the PID control variables, and the temperature deltas required for a crisp IR image could be determined. The effectiveness of the surface-mounted RTDs on the inner face of the test surface compared to non-contact IR thermocouples should be investigated if the quality of the images is not satisfactory.

Wind Tunnel Wall Liners

A proposed set of upper and lower wall liners were designed in Solidworks for the test section of the KSWT and the SWIFTER model, based on the streamlines around an infinite SWIFTER airfoil at angle of attack of negative 2^{o}, and an angle of incidence of 30^{o}, to create a zero-lift condition. The thickness of the liners was set at such that it would smoothly interface with the contraction cone fairing from the experiments involving the ASU (67)-0315 model, and avoid any potential problems with choking effects. Due to the smaller span of the SWIFTER model, an airfoil spacer was also designed to fill the gap between the lower wall liner and the root end of the model. The liners were then split into quadrants to allow them to be inserted into the test section around the SWIFTER model. To meet manufacturing limitations imposed by the standard dimensions of stock foam billets, and the maximum thickness limit of the foam cutting machine, as well as limitations based on the structural rigidity of the foam material itself, the quadrants were then broken up into an assembly of pieces which would be permanently assembled and coated in fiberglass prior to their installation in the test section. A system of nomenclature was devised to keep track of the large number of final pieces.

Preliminary Tests

An experiment was devised to develop some initial avenues of investigation in step excrescences, and to allow the test operators to gain experience. It involved using the ASU (67)-0315 model in the KSWT with a step geometry created by applying material to the test surface of the model. After comparing various options for practicality and surface finish requirements, an adhesive-backed neoprene rubber sheet material, with a layer of Kapton film across its surface was found to be most suitable. A forward-facing step configuration was selected, with a 1.6mm *k* step excrescence height. The leading edge of the step material was located at 22% chord, and extended back to aft of 65% chord. Naphthalene flow visualization was used to detect transition location. Tests were conducted at a range of chord Reynolds number values selected to produce Re_k values on the same order as the Northrop SETS tests. Due to issues with naphthalene application, and step leading edge contamination, a definitive transition front was not identified at any tested chord Reynolds number. However, images recorded did show multiple distinct wavelength structures across the span of the model, all at or below the most destructive 12mm wavelength. These may be a result of minor irregularities in the vertical face of the step.

Looking forward to testing with the SWIFTER model, it seems worthwhile to bear these wavelength structures in mind, in case they reoccur. They may be part of the step excrescence flow phenomena, or it may indicate, as was suspected with this series of

tests, that a lack of uniformity in the vertical face of the forward-facing step could be at fault, and that the Kapton film on the leading edge of the body of the SWIFTER model may need better application technique. Finally, the non-orthogonal angle of incidence of the flow on the face of the step resulting from the curvature of the surface should be calculated to create a proper correlation between the Re_k values recorded on the SWIFTER model and those in previous studies.

REFERENCES

AM Bender, M Bleazard, RV Westphal, AJ Vavra, A Drake. "An Approach to Measuring the Effects of Surface Excrescences on Transition in the Presence of Arbitrary Pressure Gradients". *Instrumentation in Aerospace Simulation Facilities*. Vol. 21, 2005, pp. 150-158.

AM Bender and A Drake. "AIR VEHICLE TECHNOLOGY INTEGRATION PROGRAM (AVTIP) Delivery Order 0020: Prediction of Manufacturing Tolerances for Laminar Flow, Task 6: Final Report" AFRL-VA-WP-TR-2007-3086. 2006.

AM Bender, A Drake, VS McKay, RV Westphal, S Yoshioka, Y Kohama. "An Approach to Measuring the Effects of Surface Steps on Transition Using a Propelled-Model". *Instrumentation in Aerospace Simulation Facilities.* Vol. 22, 2007, pp. 1-6.

IP Castro and A Haque. "The Structure of a Turbulent Shear Layer Bounding a Separation Region". *Journal of Fluid Mechanics*. Vol. 160, 1987, pp. 439-468.

JD Crouch, VS Kosorygin, LL Ng. "Modeling the Effects of Steps on Boundary-Layer Transition" *Fluid Mechanics and Its Applications*. Vol. 78, 2006, pp.37-44.

JR Dagenhart and WS Saric. "Crossflow Stability and Transition Experiments in Swept-Wing Flow". NASA TP-1999-209344, July 1999.

H Deyhle and H Bippes. "Disturbance Growth in an Unstable Three-Dimensional Boundary Layer and its Dependence on Environmental Conditions". *Journal of Fluid Mechanics.* Vol. 316, 1996, pp. 73-113.

A Drake and AM Bender. "Surface Excrescence Transition Study Delivery Order 0053: Final Report" AFRL-RB-WP-TR-2009-3109. 2009.

A Drake, AM Bender, AJ Korntheuer, RV Westphal, BJ McKeon, S Gerashchenko, W Rohe, G Dale. “Step Excrescence Effects for Manufacturing Tolerances on Laminar Flow Wings”. AIAA Paper 2010-375, Jan. 2010.

A Drake, AM Bender, RV Westphal. “Transition Due to Surface Steps in the Presence of Favorable Pressure Gradients”. AIAA Paper 2008-7334, Aug. 2008.

A Drake, RV Westphal, FA Zuniga, RA Kennelly, DJ Koga. “Wing Leading Edge Joint Laminar Flow Tests”. NASA Technical Memorandum 4762. Oct. 1996.

DM Driver, HL Seegmiller, JG Marvin. “Time-Dependent Behavior of a Reattaching Shear Layer” *AIAA Journal.* Vol. 25, No. 7, 1987, pp. 914-919.

A Fage. “The Smallest Size of a Spanwise Surface Corrugation which affects Boundary-layer Transition on an Aerofoil”. British Aeronautical Research Council Rpt. 2120. 1943.

JA Fanning. “In-Flight Measurements of Freestream Atmospheric Turbulence Intensities”. Master’s Thesis, Department of Aerospace Engineering, Texas A&M University, College Station, TX, 2012.

CW McKnight. “Design and Safety Analysis of an In-Flight, Test Airfoil”. Master’s Thesis, Department of Aerospace Engineering, Texas A&M University, College Station, TX, 2006.

CJ Obara and BJ Holmes. “Manufacturing Tolerances for Natural Laminar Flow Airframe Surfaces”. SAE Paper 850863. Apr. 1985.

RH Radetsky Jr., MS Reibert, WS Saric. “Effect of Isolated Micron-Sized Roughness on Transition in Swept-Wing Flows”. *AIAA Journal.* Vol. 37, No.11, 1999, pp. 1370-1377.

WS Saric, “Control of Transition” *Boundary Layer Stability and Transition Lecture Notes*. 2010.

WS Saric and EB White. “Influence of High-Amplitude Noise on Boundary-Layer Transition to Turbulence”. AIAA Paper 98-2645, 1998.

SN Sinha, AK Gupta, MM Oberai. “Laminar Separating Flow over Backsteps and Cavities Part II: Cavities”. *AIAA Journal*. Vol.20, No. 3, 1982, pp. 370-375.

YX Wang and M Gaster. “Effect of Surface Steps on Boundary Layer Transition” *Experiments in Fluids*, Vol. 39, 2005, pp. 679-686.

EB White. “Breakdown of Crossflow Vortices”. PhD Dissertation, Department of Mechanical and Aerospace Engineering, Arizona State University, Tempe, AZ, 2000.

D Zhou and T Wang. “Laminar Boundary Layer Flow and Heat Transfer With Favorable Pressure Gradient at Constant K Values”. ASME Paper 92-GT-246. 1992.

APPENDIX

WALL LINER PIECES AND DIMENSIONS

Extreme Dimensions of Wall Liner Pieces

Section	Part	Layer	Length (in)	Width (in)	Height (in)	Sheet Thickness (in)
Lower TS	A	1	82.0	24.5	3.0	3.0
		2	82.0	24.5	3.0	3.0
		3	26.4	5.4	1.4	1.5
	B	1a	96.0	23.6	2.0	2.0
		1b	13.5	23.6	2.0	2.0
		2a	96.0	23.6	1.5	1.5
		2b	13.5	23.6	1.5	1.5
		3a	26.7	23.6	3.0	3.0
		3b	24.0	5.2	1.8	2.0
		3c	24.0	5.9	1.8	2.0
		3d	24.0	5.9	1.9	2.0
		3e	10.8	5.8	1.9	2.0
Lower NTS	A	1	82.0	30.4	3.0	3.0
		2	82.0	30.4	2.5	2.5
		3	44.1	6.5	1.0	1.0
	B	1a	96.0	30.4	2.0	2.0
		1b	13.5	30.4	2.0	2.0
		2a	96.0	30.4	2.0	2.0
		2b	13.5	30.4	2.0	2.0
		3a	6.3	27.8	1.5	1.5
		3b-in	7.0	4.1	1.2	1.5
		3b-out	6.5	22.5	0.1	1.0
		3c	15.0	2.6	1.3	1.5
		3d	24.0	6.0	1.7	2.0
		3e	24.0	6.0	1.7	2.0
		3f	24.0	6.5	1.8	2.0
		3g	9.2	6.6	1.8	2.0

Section	Part	Layer	Length (in)	Width (in)	Height (in)	Sheet Thickness (in)
Upper TS	A	1a	96.0	24.5	2.0	2.0
		1b	18.0	24.5	2.0	2.0
		2a	96.0	24.5	1.5	1.5
		2b	18.0	24.5	1.5	1.5
		3a	93.2	24.5	2.0	2.0
		3b	22.0	22.0	2.0	2.0
		4a	92.1	24.4	1.6	2.0
		4b	22.9	21.9	2.6	3.0
	B	1	77.5	23.6	3.0	3.0
		2	77.5	23.6	3.0	3.0
		3	77.5	23.6	1.5	1.5
		4	77.5	23.5	1.7	2.0
Upper NTS	A	1a	96.0	30.4	2.0	2.0
		1b	18.0	30.4	2.0	2.0
		2a	96.0	30.4	1.5	1.5
		2b	18.0	30.4	1.5	1.5
		3a	93.2	30.4	2.0	2.0
		3b	21.9	28.1	2.0	2.0
		4a	92.1	29.6	2.1	2.5
		4b	23.2	28.2	2.8	3.0
	B	1	77.5	30.4	3.0	3.0
		2	77.5	30.4	3.0	3.0
		3	77.5	30.4	2.6	3.0
Airfoil Spacer		TS A	26.8	3.6	2.6	3.0
		TS B	28.5	3.6	2.6	3.0
		NTS A	26.8	2.2	2.6	3.0
		NTS B	25.7	2.2	2.6	3.0